nature communications

Article

https://doi.org/10.1038/s41467-025-57614-y

TET2 deficiency increases the competitive advantage of hematopoietic stem and progenitor cells through upregulation of thrombopoietin receptor signaling

Received: 22 March 2024

Accepted: 27 February 2025

Published online: 10 March 2025

Check for updates

Yitong Yang[1,2], Severine Cathelin[2], Alex C. H. Liu[1,2], Amit Subedi[2], Abdula Maher[2,3], Mohsen Hosseini[2], Dhanoop Manikoth Ayyathan[2], Robert Vanner[2] & Steven M. Chan[1,2]

Ten-Eleven Translocation-2 (*TET2*) mutations drive the expansion of mutant hematopoietic stem cells (HSCs) in clonal hematopoiesis (CH). However, the precise mechanisms by which *TET2* mutations confer a competitive advantage to HSCs remain unclear. Here, through an epigenetic drug screen, we discover that inhibition of disruptor of telomeric silencing 1-like (DOT1L), a H3K79 methyltransferase, selectively reduces the fitness of *Tet2* knockout ($Tet2^{KO}$) hematopoietic stem and progenitor cells (HSPCs). Mechanistically, we find that TET2 deficiency increases H3K79 dimethylation and expression of *Mpl*, which encodes the thrombopoietin receptor (TPO-R). Correspondingly, TET2 deficiency is associated with a higher proportion of primitive *Mpl*-expressing (Mpl^{+}) cells in the HSC compartment. Importantly, inhibition of *Mpl* expression or the signaling downstream of TPO-R is sufficient to reduce the competitive advantage of murine and human TET2-deficient HSPCs. Our findings demonstrate a critical role for aberrant TPO-R signaling in *TET2* mutation-driven CH and uncover potential therapeutic strategies against this condition.

Clonal hematopoiesis (CH) refers to a condition in which a hematopoietic stem cell (HSC) acquires genetic alterations that confer the mutant cell a competitive advantage over wild-type (WT) HSCs, resulting in its clonal expansion over time[1]. Clonal hematopoiesis of indeterminate potential (CHIP) is a more narrowly defined condition in which cancer-associated mutations are present at ≥ 2% variant allele frequency (VAF) in the blood cells of an individual without evidence of a blood cancer[2]. CHIP carriers are at a higher risk of developing hematologic malignancies and other age-related inflammatory illnesses such as cardiovascular diseases, relative to non-carriers[1,3,4].

Ten-Eleven Translocation-2 (*TET2*), which encodes a methylcytosine dioxygenase[5], is the second most frequently mutated gene in CHIP[6,7]. Loss-of-function (LoF) mutations in *TET2* are found in 10–30% of CHIP carriers[8–10]. TET2 regulates gene expression by catalyzing DNA demethylation via the conversion of 5-methylcytosine (5-mC) to 5-hydroxymethylcytosine (5-hmC)[11,12]. In murine models, TET2 deficiency increases the self-renewal of HSCs as assessed by competitive transplantation assays and leads to an expansion of the HSC compartment over time[13–16]. These findings indicate that TET2 activity is critical regulator of stemness properties in HSCs. However, the precise mechanisms by which loss of TET2 activity leads to the competitive advantage of *TET2*-mutated HSCs remain elusive.

To uncover potential mechanisms, we performed an epigenetic drug screen to identify differential dependencies between *Tet2*

[1]Department of Medical Biophysics, Temerty Faculty of Medicine, University of Toronto, Toronto M5G 1L7, Canada. [2]Princess Margaret Cancer Centre, University Health Network, Toronto M5G 1L7, Canada. [3]Institute of Medical Science, Temerty Faculty of Medicine, University of Toronto, Toronto M5S 1A8, Canada. e-mail: steven.chan@uhn.ca

knockout (KO) and *Tet2* wildtype (WT) hematopoietic progenitor cells (HPCs). Through this screen and subsequent mechanistic studies, we discovered that aberrant thrombopoietin receptor (TPO-R) signaling plays a critical role in promoting the competitive advantage of TET2-deficient HSPCs.

Results

Chemical library screen reveals a dependency on DOT1L activity in *Tet2*^{KO} HPCs

To identify potential differential dependencies between *Tet2*^{KO} and *Tet2*^{WT} HPCs, we first generated an isogenic cell line system by over-expressing human Homeobox B4 (HOXB4), a transcription factor involved in self-renewal of stem cells[17], and a fluorescent reporter (Venus) in Sca-1$^+$ bone marrow (BM) cells isolated from a *Tet2*^{KO} mouse and a sex-matched *Tet2*^{WT} littermate (Supplementary Fig. 1A, B)[16]. Overexpression of HOXB4 has been shown to immortalize murine HPCs without frank leukemic transformation[18]. The resulting cells (hereafter referred to as HPC^{HOXB4}) could be grown indefinitely in cytokine supplemented medium and displayed a granulocyte-monocyte progenitor (GMP)-like surface immunophenotype (Lin$^-$ / Sca-1$^-$ / c-Kit$^+$ / CD34$^+$ / CD16/32$^+$) (Supplementary Fig. 1C). The immunophenotype profiles were similar between *Tet2*^{WT} and *Tet2*^{KO} HPC^{HOXB4} cells (Supplementary Fig. 1C). The *Tet2*^{KO}HPC^{HOXB4} cells demonstrated a strong competitive growth advantage over *Tet2*^{WT}HPC^{HOXB4} cells in culture (Fig. 1A). This finding is consistent with previous studies showing that TET2 deficiency confers a repopulating advantage to not only HSCs but also committed progenitors, including GMPs and neutrophil progenitors[19,20].

Given the epigenetic role of TET2, we reasoned that its deficiency could be associated with dependencies on the activity of other

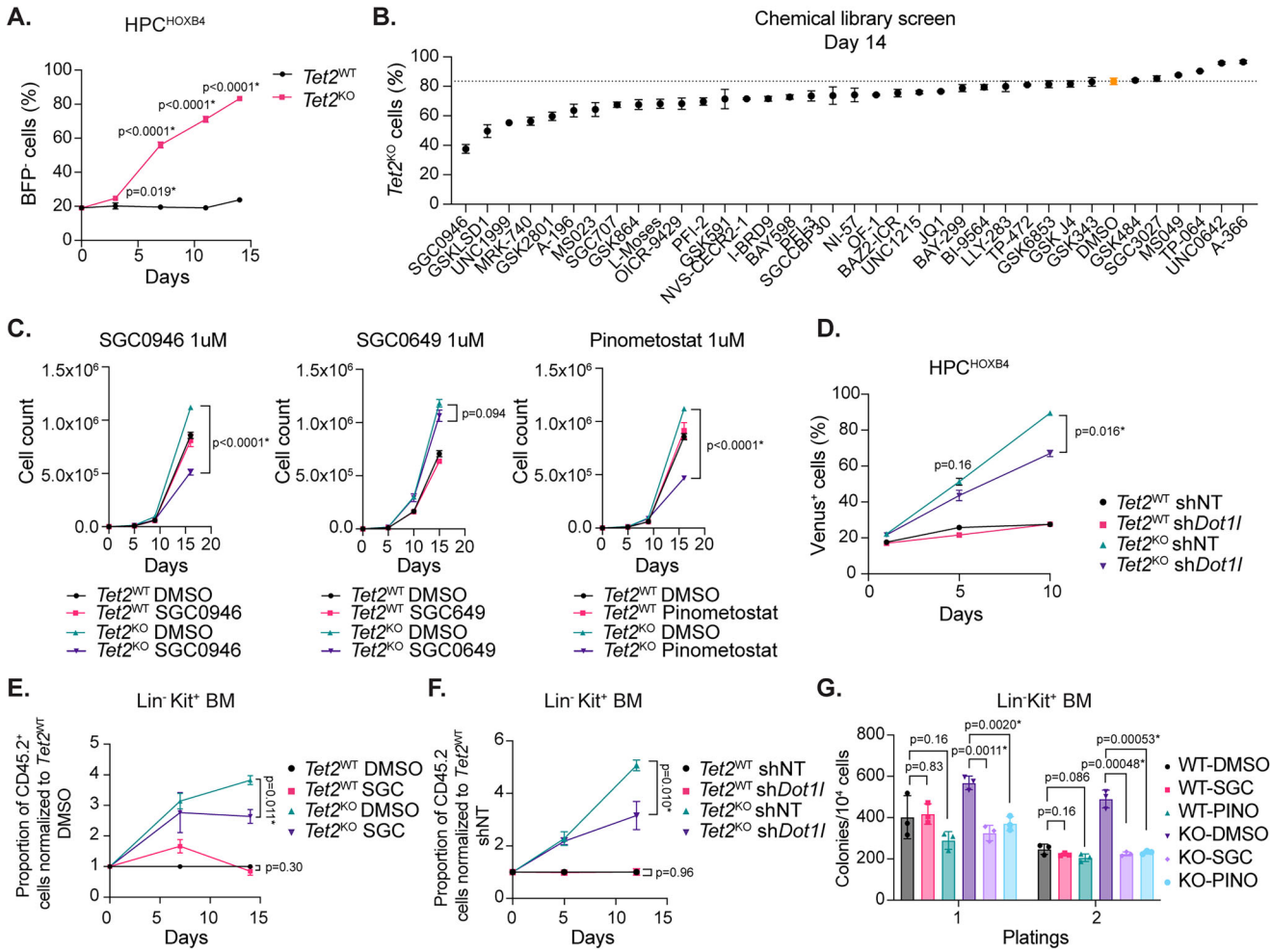

Fig. 1 | *Tet2*^{KO} HSPCs are dependent on DOT1L activity. A Percentage of BFP$^-$*Tet2*^{WT} or BFP$^-$*Tet2*^{KO} HPC^{HOXB4} cells in competition with BFP$^+$*Tet2*^{WT} HPC^{HOXB4} cells at the indicated time points after starting the experiment. $n = 3$ experimental replicates. Unpaired t test used for significance. **B** The percentage of BFP$^-$*Tet2*^{KO} HPC^{HOXB4} cells after treatment with the indicated compounds or DMSO (highlighted in orange) for 14 days. The dashed line represents the percentage of *Tet2*^{KO} HPC^{HOXB4} in DMSO treatment. Data represent the average of 3 experimental replicates. Representative data from one of 3 independent screens are shown. **C** Count of Annexin V negative *Tet2*^{KO} or *Tet2*^{WT} HPC^{HOXB4} cells treated with 1 µM of each compound over time normalized to the corresponding untreated sample. $n = 3$ experimental replicates. Unpaired t test with multiple testing corrections used for significance. **D** Percentage of Venus$^+$*Tet2*^{WT} or Venus$^+$*Tet2*^{KO} HPC^{HOXB4} cells in competition with Venus$^-$*Tet2*^{WT} HPC^{HOXB4} cells over time. Both cell types were transduced with the indicated shRNA vectors. $n = 3$ experimental replicates. Unpaired t test used for significance. **E** Proportion of CD45.2$^+$*Tet2*^{KO} or CD45.2$^+$*Tet2*^{WT} HSPCs in competition with CD45.1$^+$*Tet2*^{WT} HSPCs after treatment with DMSO or SGC0946 (SGC; 1 µM). Data are normalized to DMSO-treated CD45.2$^+$*Tet2*^{WT} cells. Unpaired t test used for significance. $n = 3$ experimental replicates. **F** Proportion of CD45.2$^+$*Tet2*^{KO} or CD45.2$^+$*Tet2*^{WT} HSPCs in competition with CD45.1$^+$*Tet2*^{WT} HSPCs gated on the transduced BFP$^+$ population. Data are normalized to shNT-expressing CD45.2$^+$*Tet2*^{WT} cells. Unpaired t test used for significance. $n = 3$ experimental replicates. Data are shown as mean ± SEM. **G** Number of colonies formed in per 1×10^4 Lin$^-$Kit$^+$ (LK) HSPCs in the presence of DMSO or SGC0946 (SGC; 1 µM). $n = 3$ experimental replicates. Unpaired t test used for significance. All data shown are mean ± SD unless otherwise indicated. Asterisks indicate statistical significance. Source data are provided as a Source Data file.

epigenetic regulators. Therefore, we used the isogenic cell lines to conduct a drug screen of 36 well-characterized and specific epigenetic chemical probes from the Structural Genomics Consortium (SGC)[21]. To conduct the screen, *Tet2*^{KO}HPC^{HOXB4} cells were mixed at a 1:4 ratio with *Tet2*^{WT}HPC^{HOXB4} competitor cells that were marked by blue fluorescent protein (BFP) expression. The mixed population was then treated with each probe for 14 days (Supplementary Fig. 1D). The screen identified SGC0946, an inhibitor of the activity of histone H3 at lysine 79 (H3K79) methyltransferase disruptor of telomeric silencing 1-like (DOT1L)[22], as the top compound that reduced the competitive advantage of *Tet2*^{KO}HPC^{HOXB4} cells (Fig. 1B). Treatment with SGC0946, but not the inactive control compound SGC0649, selectively decreased the growth of *Tet2*^{KO}HPC^{HOXB4} cells by reducing their viability and cell proliferation (Fig. 1C, Supplementary Fig. 1E, F). A similar impact on *Tet2*^{KO}HPC^{HOXB4} cells was observed with pinometostat, another DOT1L inhibitor (Fig. 1C, Supplementary Fig. 1E, F)[23]. To determine if DOT1L inhibition impacted the differentiation status of HPC^{HOXB4} cells, we measured the expression of the myeloid differentiation markers, CD11b and CD16/32, at baseline and after SGC0946 treatment. *Tet2*^{KO}HPC^{HOXB4} cells expressed lower levels of the markers than *Tet2*^{WT}HPC^{HOXB4} at baseline (Supplementary Fig. 1G), a finding consistent with prior studies[16,24]. SGC0946 treatment increased CD11b and CD16/32 expression on both *Tet2*^{WT} and *Tet2*^{KO} HPC^{HOXB4} (Supplementary Fig. 1G). This finding aligns with prior studies showing that DOT1L inhibition increases the expression of mature myeloid markers in *KMT2A*-rearranged leukemia[25,26]. Importantly, SGC0946 treatment increased the expression of these markers to a greater extent on *Tet2*^{KO} than *Tet2*^{WT} HPC^{HOXB4} cells (Supplementary Fig. 1G), suggesting that DOT1L activity is required for maintaining the less differentiated state of *Tet2*^{KO} HPC^{HOXB4} cells.

To further validate these findings, we downregulated *Dot1l* expression using RNA interference (RNAi) (Supplementary Fig. 1H) and observed a selective reduction in the competitive advantage of *Tet2*^{KO}HPC^{HOXB4} cells (Fig. 1D). DOT1L inhibitor treatment or genetic knockdown of *Dot1l* also selectively reduced the competitive advantage (Fig. 1E, F and Supplementary Fig. 1H) and clonogenic potential of unmodified *Tet2*^{KO} Lin^{-} / c-Kit^{+} (LK) BM cells (Fig. 1G and Supplementary Fig. 1I), indicating that the dependency on DOT1L was not an artifact of HOXB4 overexpression. Together, our findings indicate that TET2-deficient HPCs are dependent on DOT1L activity to maintain their competitive advantage over WT HPCs.

TET2 deficiency increases DOT1L-mediated H3K79 dimethylation of the *Mpl* locus and *Mpl* gene expression in HPCs

To identify candidate genes that mediate this differential effect and further explore the transcriptomic alterations driven by TET2 deficiency, we performed bulk RNA sequencing (RNA-seq) and H3K79 dimethylation (H3K79me2) chromatin immunoprecipitation followed by sequencing (ChIP-seq) analyses on untreated and SGC0946-treated *Tet2*^{KO} and *Tet2*^{WT} HPC^{HOXB4} cells. The RNA-seq analysis revealed 598 differentially upregulated genes in *Tet2*^{KO} cells relative to *Tet2*^{WT} cells and 70 differentially downregulated genes in SGC0946-treated *Tet2*^{KO} cells relative to untreated *Tet2*^{KO} cells (Fig. 2A and Supplementary Data 1). Twenty genes overlapped between these two sets (Fig. 2B, C). Pathway enrichment analysis of the differentially upregulated genes between *Tet2*^{KO} versus *Tet2*^{WT} HPC^{HOXB4} cells revealed an enrichment of pathways associated with inflammatory cytokine signaling in *Tet2*^{KO}HPC^{HOXB4} cells (Supplementary Fig. 2A and Supplementary Data 2), in line with the previously reported association between TET2 deficiency and inflammation[27–29].

Next, we analyzed for potential differences in H3K79 methylation at the global and locus-specific level between *Tet2*^{KO} and *Tet2*^{WT} HPC^{HOXB4} cells. Total H3K79me2, H3K79me3, and DOT1L proteins levels as determined by Western blotting were similar between these two cell types (Supplementary Fig. 2B, C). ChIP-seq analysis also showed that genome-wide levels and distribution of H3K79me2 were similar between untreated *Tet2*^{KO} and *Tet2*^{WT}HPC^{HOXB4} cells (Fig. 2D). As anticipated, treatment with SGC0946 decreased the level of H3K79me2 in both *Tet2*^{KO} and *Tet2*^{WT} HPC^{HOXB4} cells (Fig. 2D and Supplementary Fig. 2B). However, the magnitude of decrease was greater in *Tet2*^{KO} cells, which could be due to their higher proliferation rate resulting in faster passive dilution of H3K79me2 marks (Supplementary Fig. 1F). Differential H3K79me2 methylation analysis at the locus-specific level revealed that TET2 deficiency was associated with both increases and decreases in H3K79me2 across genomic regions in roughly equal proportions (Supplementary Fig. 2D and Supplementary Data 3). This observation aligns with our other findings demonstrating no global alterations in H3K79me2 levels. In contrast, SGC0946 treatment induced hypomethylation of the majority of differentially methylated regions in both *Tet2*^{WT} and *Tet2*^{KO} cells, with a more pronounced effect observed in *Tet2*^{KO} cells (Supplementary Fig. 2D and Supplementary Data 3). Pathway enrichment analysis using KEGG pathway gene sets revealed that the JAK-STAT signaling pathway was the most significantly enriched among H3K79-hypermethylated genes in *Tet2*^{KO}HPC^{HOXB4} cells compared with their *Tet2*^{WT} counterparts (Supplementary Fig. 2E). Further analysis of the H3K79-hypermethylated genes in the JAK-STAT signaling pathway gene set revealed genes involved in key cellular processes that might play a role in promoting the competitive advantage of *Tet2*^{KO} cells (Supplementary Fig. 2F). These include genes involved in positive regulation of cell cycle progression such as cyclin D genes (*Ccnd1*, *Ccnd2*, and *Ccnd3*)[30]. Additionally, increased H3K79 methylation was observed at genes encoding inflammatory cytokine receptors (*Il6ra* and *Il15ra*), which could potentially exacerbate inflammatory responses[31,32]. These findings collectively indicate that DOT1L-mediated H3K79 hypermethylation at specific loci may contribute to the competitive advantage of TET2-deficient cells.

Given that H3K79me2 is correlated with active gene transcription[33], we reasoned that the candidate genes should be more highly expressed and associated with higher H3K79me2 levels in *Tet2*^{KO} cells relative to *Tet2*^{WT} cells. Furthermore, their gene expression and associated H3K79me2 levels should be reduced with DOT1L inhibition. Differential H3K79me2 analysis at the locus-specific level identified 744 genes with increased methylation in *Tet2*^{KO} cells relative to *Tet2*^{WT} cells, 4,324 genes with decreased methylation in SGC0946-treated *Tet2*^{KO} cells relative to untreated *Tet2*^{KO} cells, and 357 overlapping genes between these two sets (Fig. 2E and Supplementary Fig. 2G). Intriguingly, the intersection between the 4 sets of genes defined by differential gene expression and H3K79me2 levels contained only two genes, *St8sia6* and *Mpl* (Fig. 2F), which encode a sialyltransferase and a receptor for the cytokine, thrombopoietin (TPO), respectively[34–36]. We decided to focus on the role of *Mpl* in our subsequent studies because 1) *Mpl* was more significantly differentially expressed than *St8sia6* (Supplementary Fig. 2H, I) and 2) TPO signaling has been shown to regulate hematopoietic stem cell (HSC) self-renewal and expansion[37–39]. Quantitative RT-PCR analysis confirmed that Mpl expression was significantly higher in *Tet2*^{KO} compared with *Tet2*^{WT} cells at baseline and decreased after SGC0946 treatment in both HPC^{HOXB4} and unmodified LK BM cells (Fig. 2G). The changes in gene expression were associated with a higher level of H3K79me2 at the body and promoter region of the *Mpl* gene in *Tet2*^{KO} relative to *Tet2*^{WT} HPC^{HOXB4} cells and a decrease in the histone mark after SGC0946 treatment (Fig. 2H). To confirm that this finding was not restricted to HOXB4-overexpressing cells, we conducted ChIP-qPCR analysis of unmodified LK BM cells and observed a higher enrichment of H3K79me2 at the *Mpl* locus in *Tet2*^{KO} than *Tet2*^{WT} cells (Supplementary Fig. 2J).

https://doi.org/10.1038/s41467-025-57614-y

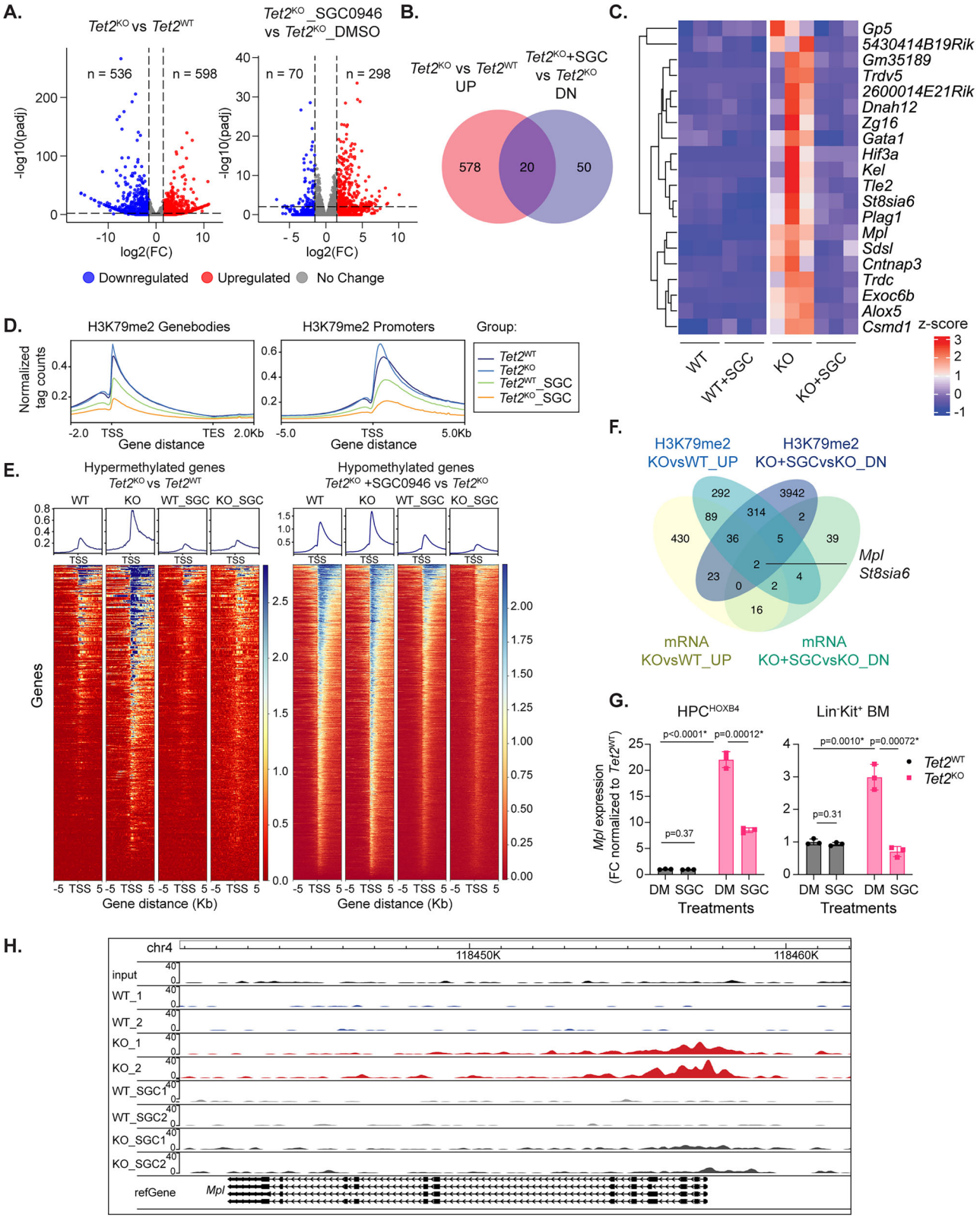

To investigate whether DOT1L-mediated H3K79 methylation of the *Mpl* locus is sufficient to upregulate its expression, we transduced *Tet2*^{WT}HPC^{HOXB4} cells with lentiviral vectors expressing sgRNAs targeting the murine *Mpl* promoter and gene body regions (P + G), or a non-targeting (NT) control sgRNA. We then transfected these cells with a vector expressing the dCas9-DOT1L fusion protein, which has previously been shown to increase expression of target genes through H3K79 methylation[40]. At 72 hours post-transfection, HPC^{HOXB4} cells harboring the *Mpl*-targeting sgRNAs expressed higher levels of *Mpl* compared to those with control sgRNA (Supplementary Fig. 2K), suggesting that DOT1L-mediated H3K79 methylation of the *Mpl* locus is sufficient to upregulate its expression. Taken together, these findings provide evidence that TET2 deficiency causes aberrant H3K79 hypermethylation at the *Mpl* locus and a consequent increase in *Mpl* gene expression.

Fig. 2 | *Mpl* expression is upregulated and associated with increased H3K79me2 at the gene locus in *Tet2*^{KO} HSPCs. A Volcano plots of differentially expressed genes (DEGs) comparing *Tet2*^{KO} versus *Tet2*^{WT} HPC^{HOXB4} cells and SGC0946-treated versus untreated *Tet2*^{WT} HPC^{HOXB4} cells. **B** Venn diagram showing the overlap of DEGs upregulated in *Tet2*^{KO} cells and downregulated in SGC0946-treated *Tet2*^{KO} cells. **C** Heatmap showing the z-scaled normalized read counts of the 20 overlapping genes in (**B**). **D** Distribution of H3K79me2 signals at the transcription start site (TSS) and gene body. Each curve represents data randomly sampled from two replicates in the same group. **E** Distribution of H3K79me2 signals centered around the TSS of differentially methylated genes of each indicated pairwise comparison. The values in each row represent data randomly sampled from two replicates. **F** Venn diagram showing the overlap between the 4 sets of genes defined by differential gene expression and H3K79me2 levels. **G** *Mpl* gene expression by RT-qPCR in HPC^{HOXB4} cells and unmodified Lin$^-$Kit$^+$ HSPCs treated either with DMSO (DM) or SGC0946 (SGC, 1 μM) for 7 days. Ct values were normalized to *Actb*. Expression was shown as FC normalized to *Tet2*^{WT}. $n = 3$ experimental replicates. Unpaired t test used for significance. **H** Genome browser view of H3K79me2 signals at the *Mpl* locus in HPC^{HOXB4} cells ($n = 2$ biological replicates). Data shown are mean ± SD. Asterisks indicate statistical significance. Source data are provided as a Source Data file.

TET2 deficiency increases the proportion of *Mpl*$^+$ cells in the HSC compartment

Mpl expression in HSCs has previously been shown to be associated with stemness properties including self-renewal, quiescence, and long-term repopulation potential[41,42]. Based on these and our findings above, we hypothesized that a potential mechanism by which TET2 deficiency confers a competitive advantage to mutant HSCs is through increased *Mpl* expression in the HSC compartment in a DOT1L-dependent manner. To test this hypothesis, we transplanted *Tet2*^{WT} or *Tet2*^{KO} whole BM cells from sex-matched littermates in a non-competitive manner into lethally irradiated mice. At 4 weeks after transplantation, we treated the engrafted mice with vehicle or pinometostat at 60 mg/kg twice a day by subcutaneous injection ($n = 2$ of each treatment condition and genotype). This in vivo dosing regimen has previously been reported to reduce H3K79 methylation and suppress tumor growth in mice[43]. After 21 days of treatment, we isolated LK BM cells from the recipients and performed single cell RNA-seq (scRNA-seq) analysis (Fig. 3A)[44,45]. Pinometostat treatment reduced the global level of H3K79me2 by ~60% in the LK BM cells (Supplementary Fig. 3A, B). Data integration and clustering analysis of the scRNA-seq data identified 27 transcriptional clusters and nine stem and progenitor fractions according to a murine HSPC gene expression reference dataset (Fig. 3B)[46,47]. The clustering pattern was similar between *Tet2*^{KO} and *Tet2*^{WT} cells (Supplementary Fig. 3C). Consistent with prior studies, the proportion of transcriptomically-defined HSCs was higher in *Tet2*^{KO} LK BM than that in *Tet2*^{WT} cells (Fig. 3C and Supplementary Fig. 3D)[47–49]. Pinometostat treatment reduced the proportion of HSCs in *Tet2*^{KO} samples to a level comparable to that of untreated *Tet2*^{WT} samples (Fig. 3C and Supplementary Fig. 3D). Among the transcriptomically-defined HSC subsets, the impact of TET2 deficiency and pinometostat was most pronounced in the HSC-1 cluster (Fig. 3D). Cells in the HSC-1 cluster exhibited the highest enrichment scores for two stemness-related gene signatures among the three clusters, suggesting that it is the most primitive population (Supplementary Fig. 3E). These findings suggest that the expansion of HSCs due to TET2 deficiency is at least partially dependent on DOT1L activity.

Gene signature analysis revealed an enrichment of genes associated with stemness and quiescence in *Tet2*^{KO} cells compared with *Tet2*^{WT} cells in the HSC-1 cluster (Supplementary Fig. 3E), suggesting that TET2 deficiency might increase the proportion of a more primitive subset of cells in the heterogeneous transcriptomically-defined HSC-1 cluster. Since we found that TET2 deficiency upregulated *Mpl* expression, which has previously to shown to be a marker of long-term HSCs (LT-HSCs)[42], we analyzed the pattern of *Mpl* expression in our scRNA-seq dataset. *Mpl* expression was mostly restricted to cells in the HSC and megakaryocyte progenitor (MkP) clusters (Fig. 3E). Notably, the proportion of cells with any detectable *Mpl* transcript in the HSC clusters was higher in *Tet2*^{KO} than in *Tet2*^{WT} samples (Fig. 3F). To confirm this finding, we employed a more stringent threshold of ≥3 detectable *Mpl* transcripts to define high *Mpl* expression (*Mpl*^{Hi}). The proportion of *Mpl*^{Hi} cells in the HSC-1 cluster was significantly higher in *Tet2*^{KO} than in *Tet2*^{WT} samples, a difference that was abrogated by pinometostat treatment (Fig. 3G and Supplementary Fig. 3F). Pinometostat did not decrease *Mpl* expression in MkPs, indicative of a cell-type specific drug effect (Supplementary Fig. 3F). To determine if *Mpl* expression was associated with a more primitive subset of HSCs in our dataset, we performed gene set enrichment and differential gene expression analyses comparing the *Mpl*$^+$ versus *Mpl*$^-$ fraction in the transcriptionally defined HSC clusters of vehicle-treated samples[50,51]. These analyses revealed an upregulation of genes associated with stemness (e.g., *Hoxb5*, *Mycn*, and *Mecom*) and downregulation of genes associated with lineage commitment (e.g., *Mpo* and *Csf1r*) in the *Mpl*$^+$ fraction compared with the *Mpl*$^-$ fraction in the HSC-1 cluster (Fig. 3H, I), providing evidence that the *Mpl*$^+$ fraction was more primitive than the *Mpl*$^-$ fraction in this cluster. Importantly, the expression of stemness-related genes was similar between the *Mpl*$^+$ fraction in *Tet2*^{WT} versus *Tet2*^{KO} samples (Fig. 3H, I and Supplementary Fig. 3G), suggesting that while TET2 deficiency increases the proportion of *Mpl*-expressing cells, it does not further alter the stemness properties of the *Mpl*$^+$ cell fraction. A similar trend was observed in the HSC-2 and HSC-3 clusters, but the magnitude of difference between the *Mpl*$^+$ and *Mpl*$^-$ fractions was less pronounced in these clusters (Supplementary Fig. 3H). Re-analysis of an independent published scRNA-seq dataset comparing *Tet2*^{KO} and *Tet2*^{WT} Lin$^-$ BM cells also revealed an association between *Mpl* expression and stemness gene signatures within the HSC-1 cluster (Supplementary Fig. 3I)[47]. Together, these findings demonstrate that TET2 deficiency increases the primitive *Mpl*$^+$ cell fraction in the HSC compartment.

To further evaluate the effect of DOT1L inhibition on *Tet2*^{KO} HSCs in vivo, we conducted a competitive secondary transplant experiment (Supplementary Fig. 3J)[52]. We mixed CD45.2$^+$ *Tet2*^{WT} or *Tet2*^{KO} whole BM cells with CD45.1$^+$ *Tet2*^{WT} competing cells at a 3:7 ratio and transplanted the mixed cells into lethally irradiated recipients. After engraftment, the animals were treated with pinometostat or vehicle for 3 weeks (same duration of treatment as the scRNA-seq experiment). After the 3-week treatment period, we collected the BM cells from primary recipients and analyzed the HSC and progenitor compartments by flow cytometry. Pinometostat treatment selectively reduced the proportion of immunophenotypic HSCs (LSK / CD150$^+$ / CD48$^-$) and MPPs (LSK / CD150$^-$ / CD48$^-$) in the *Tet2*^{KO} LSK fraction but not in the *Tet2*^{WT} LSK fraction of primary transplant recipients (Fig. 3J). Pinometostat treatment also suppressed the competitive advantage of *Tet2*^{KO} cells in the HSC and MPP compartments in primary recipients (Supplementary Fig. 3K). To assess the functional impact of DOT1L inhibition on *Tet2*^{KO} HSCs, we sorted the LSK fraction from primary recipients, mixed them with supporting whole BM cells from CD45.1$^+$ *Tet2*^{WT} donors, and transplanted the mixed population into lethally irradiated secondary recipients. Three weeks after transplantation, we analyzed BM samples from the secondary recipients to assess the size and chimerism levels of different HSPC fractions. Pinometostat treatment selectively reduced the proportion of immunophenotypic HSCs the *Tet2*^{KO} LSK fraction but not in the *Tet2*^{WT} LSK fraction of secondary recipients (Supplementary Fig. 3L). *Tet2*^{KO} HSCs and progenitors also significantly outcompeted their *Tet2*^{WT} counterparts, and pinometostat treatment of primary recipients was sufficient to suppress their competitive advantage (Fig. 3K). Notably, this suppressive effect was specific to *Tet2*^{KO} cells and was not observed in *Tet2*^{WT} cells (Fig. 3K). These findings, combined with our scRNA-seq results, suggest that the

https://doi.org/10.1038/s41467-025-57614-y

competitive advantage of *Tet2*^{KO} HSCs over WT cells is, at least partially, dependent on DOT1L activity.

TET2-deficient HSPCs are dependent on thrombopoietin receptor signaling to maintain their competitive advantage

The thrombopoietin receptor (TPO-R), encoded by *Mpl*, has previously been shown to not only be a marker of LT-HSCs but also play a functional role in preserving the stemness properties of LT-HSCs and promoting their expansion through its downstream signaling pathways upon TPO activation[42,53,54]. Based on these considerations, we hypothesized that TET2 deficiency could endow a greater proportion of HSCs with the ability to respond to TPO, thereby enhancing the competitive advantage of mutant HSCs over WT HSCs. To test this hypothesis, we performed an in vitro competition experiment in which

Fig. 3 | DOT1L enhances self-renewal of *Tet2*^{KO} HSCs through differentially regulating *Mpl* expression. A Schematic diagram of scRNA-seq on *Tet2*^{WT} and *Tet2*^{KO} Lin$^-$Kit$^+$ HSPCs. Created in BioRender[84]. **B** Dimensionality reduction using Uniform Manifold Approximation and Projection (UMAP) on all the filtered cells ($n = 68{,}538$). **C** Proportion of progenitor lineages of each genotype and treatment group averaged from two biological replicates. VEH: vehicle. PINO: pinometostat. **D** Proportion of individual HSC clusters normalized to the total cell number in each sample. Data shown are mean ± SD. Significance levels shown represent two-sided Fisher's exact test results using the sum of raw counts from two biological replicates. **E** Scatterplot of cells with detected *Mpl* transcripts (red) and cells with no *Mpl* detected (gray) grouped by genotype and treatment. Two biological replicates were merged. **F** Percent of cells with detected *Mpl* transcripts in vehicle-treated samples grouped by genotype. **G** Percent of *Mpl*-high HSCs among all HSCs of each group. p values were calculated through two-sided Fisher's exact test using the sum of two replicates. Raw counts are shown in table S3F. **H** AUC enrichment score of *Mpl*-expressing (*Mpl*$^+$) and non-expressing (*Mpl*$^-$) vehicle-treated HSCs from HSC-1 for each gene set. The lower and upper hinges of the box represent the 25th and 75th percentiles, and the whiskers extend to the minimum and maximum values within 1.5 times the interquartile range. The median value is depicted by the line within the box. $n = 532$ for *Tet2*^{WT}*Mpl*$^+$; $n = 1{,}855$ for *Tet2*^{WT}*Mpl*$^-$; $n = 1{,}184$ for *Tet2*^{KO}*Mpl*$^+$; $n = 2574$ for *Tet2*^{KO}*Mpl*$^-$. Unpaired t test used for significance. **I** Heatmap showing normalized expression of differentially expressed ($|\mathrm{Log_2FC}| > 1$, padj <0.01) HSC and progenitor markers in HSCs from HSC-1 cluster grouped by *Mpl* status and genotype. **J** Percentage of each stem and progenitor fraction in CD45.2$^+$ LSK BM from primary recipients at the endpoint. $n = 5$ biological replicates per group. Data shown are mean ± SD. Unpaired t test with multiple testing correction using Holm–Sidak method used for significance. **K** Percentage of CD45.2$^+$ BM cells in each stem and progenitor population in secondary transplant recipients three weeks following transplantation. Data shown are mean ± SD. $n = 5$ biological replicates per group. Unpaired t test used for significance. Asterisks indicate statistical significance. Source data are provided as a Source Data file.

Mpl was knocked down in both CD45.2$^+$*Tet2*^{KO} and CD45.1$^+$*Tet2*^{WT} Lin$^-$ BM cells through RNAi and observed a reduction in the competitive advantage of *Tet2*^{KO} cells in the Lin$^-$, LK, and LSK fractions (Fig. 4A). A similar finding was observed using *Tet2*^{KO} and *Tet2*^{WT} HPC^{HOXB4} cells in competition assays (Supplementary Fig. 4A).

Given the challenges in assessing HSC activity in vitro, we performed an in vivo competition experiment in which we mixed CD45.1$^+$*Tet2*^{WT} and CD45.2$^+$*Tet2*^{KO} Lin$^-$ BM cells, transduced them with a lentiviral vector expressing a doxycycline-inducible non-targeting (NT) or *Mpl*-targeting shRNA, and transplanted the mixed population into lethally irradiated murine recipients (Fig. 4B and Supplementary Fig. 4B)[55]. Three weeks after transplantation, we determined the baseline level of chimerism in the transduced peripheral blood (PB) cell population and induced shRNA expression with the addition of doxycycline in drinking water. After 17 weeks of doxycycline treatment (20 weeks post-transplantation), *Mpl* knockdown reduced the proportion of CD45.2$^+$*Tet2*^{KO} PB cells relative to baseline, whereas the proportion of CD45.2$^+$*Tet2*^{KO} PB cells expressing NT shRNA increased over the same period (Fig. 4C). The CD45.2$^+$ *Tet2*^{KO} fraction exhibited a significantly higher proportion of myeloid cells compared to the CD45.1$^+$ *Tet2*^{WT} fraction (Supplementary Fig. 4C), consistent with the known myeloid differentiation bias induced by TET2 deficiency[10,56–58]. Notably, *Mpl* knockdown did not significantly reduce the proportion of myeloid cells in the transduced CD45.2$^+$ *Tet2*^{KO} fraction (Supplementary Fig. 4C). These findings suggest that the increased *Mpl* expression associated with TET2 deficiency primarily enhances the competitive advantage of HSCs rather than directly promoting myeloid lineage bias.

At 20 weeks after transplantation, the majority of PB cells should have originated from the transplanted donor's HSCs[59]. Therefore, our finding that *Mpl* silencing reduced the proportion of CD45.2$^+$ *Tet2*^{KO} PB cells suggests an impact at the level of HSCs. To further support this notion, we determined the proportion of immunophenotypic HSCs (LSK / CD150$^+$ / CD48$^-$) in the transduced LK BM cell fraction at 20 weeks after transplantation. We observed a higher proportion of immunophenotypic HSCs in the CD45.2$^+$ *Tet2*^{KO} LK fraction than in the CD45.1$^+$ *Tet2*^{WT} LK fraction (Fig. 4D). This observation is consistent with prior reports demonstrating that TET2 deficiency causes an expansion of the HSC compartment[16]. Importantly, *Mpl* knockdown reduced the proportion of HSCs in the mutant LK fraction to a level comparable to that of the control WT LK fraction (Fig. 4D). Together, these findings suggest that the higher expression of *Mpl* in *Tet2*^{KO} HSCs contributes, at least in part, to their competitive advantage over WT HSCs.

Inhibition of TPO-R/JAK2 signaling reduces the competitive advantage of murine and human TET2-deficient HSPCs

Upon ligand (TPO) binding, the TPO-R dimerizes and activates Janus Kinase 2 (JAK2), an intracellular tyrosine kinase that is associated with the cytoplasmic domain of the receptor[60]. JAK2 activation, in turn, triggers a cascade of signaling events including the phosphorylation and nuclear import of Signal Transducer and Activator of Transcription 5 (STAT5), which plays a critical role in HSC maintenance and self-renewal[61,62]. Although direct TPO-R antagonists have not been developed, JAK2 inhibitors are available and have been in clinical use for the treatment of myelofibrosis, polycythemia vera, graft-versus-host disease, and several autoimmune conditions[63–65]. Therefore, we decided to test if pharmacologic inhibition of JAK2 activity would reduce the competitive advantage of TET2-deficient HSPCs. Ruxolitinib, fedratinib, and AZ960 are potent JAK2 inhibitors with 50% inhibitory concentrations (IC_{50}) of <3 nM in cell-free enzymatic assays[66–68]. Treatment with these compounds at sub-micromolar concentrations for 7 days effectively reduced the competitive advantage of *Tet2*^{KO}HPC^{HOXB4} cells over *Tet2*^{WT}HPC^{HOXB4} cells (Supplementary Fig. 4D). Ruxolitinib treatment also selectively reduced the competitive advantage and clonogenic capacity of *Tet2*^{KO} Lin$^-$ BM cells, indicating that the drug effect was not dependent on HOXB4 overexpression (Fig. 4E, F).

To further examine the significance of JAK2 signaling, we compared the activation of STAT5 between *Tet2*^{KO} and *Tet2*^{WT} cells. We starved HPC^{HOXB4} cells of TPO for 4 hours and then stimulated them with TPO for 15 minutes. We found that TPO stimulation increased STAT5 phosphorylation only in *Tet2*^{KO}HPC^{HOXB4} cells but not in *Tet2*^{WT} HPC^{HOXB4} cells, an effect that was abolished by pre-treatment with SGC0946 or ruxolitinib (Supplementary Fig. 4E). Importantly, TPO stimulation also induced higher STAT5 phosphorylation in unmodified *Tet2*^{KO} LK BM cells (Fig. 4G), indicating that this response was not dependent on HOXB4 overexpression. To assess the effect of TET2 deficiency and DOT1L inhibition on STAT5 target gene expression, we performed gene set enrichment analysis of our scRNA-seq data using STAT5 target gene sets. This analysis revealed an upregulation of STAT5A and STAT5B target gene expression in *Tet2*^{KO} LK cells compared to *Tet2*^{WT} cells (Fig. 4H). Notably, these target genes were downregulated following pinometostat treatment (Fig. 4H). Together, these results demonstrate that TET2 deficiency augments STAT5 signaling through the TPO-R/JAK2 signaling axis.

To explore the translational relevance of our findings, we tested the effect of ruxolitinib treatment on the competitive advantage of *Tet2*^{KO} HSPCs in vivo. We mixed CD45.2$^+$*Tet2*^{KO} whole BM cells with CD45.1$^+$*Tet2*^{WT} competitor cells at a 3:7 ratio and transplanted the mixed cell population into lethally irradiated recipients. At 3 weeks post-transplantation, we determined the baseline level of chimerism in PB and randomized the mice to receive treatment with ruxolitinib at 60 mg/kg twice a day or vehicle by oral administration for 13 weeks (Fig. 4I)[69]. The proportion of CD45.2$^+$ *Tet2*^{KO} cells in PB between the treatment groups was similar at baseline (Supplementary Fig. 4F). Ruxolitinib treatment reduced STAT5 phosphorylation in CD45.2$^+$

https://doi.org/10.1038/s41467-025-57614-y

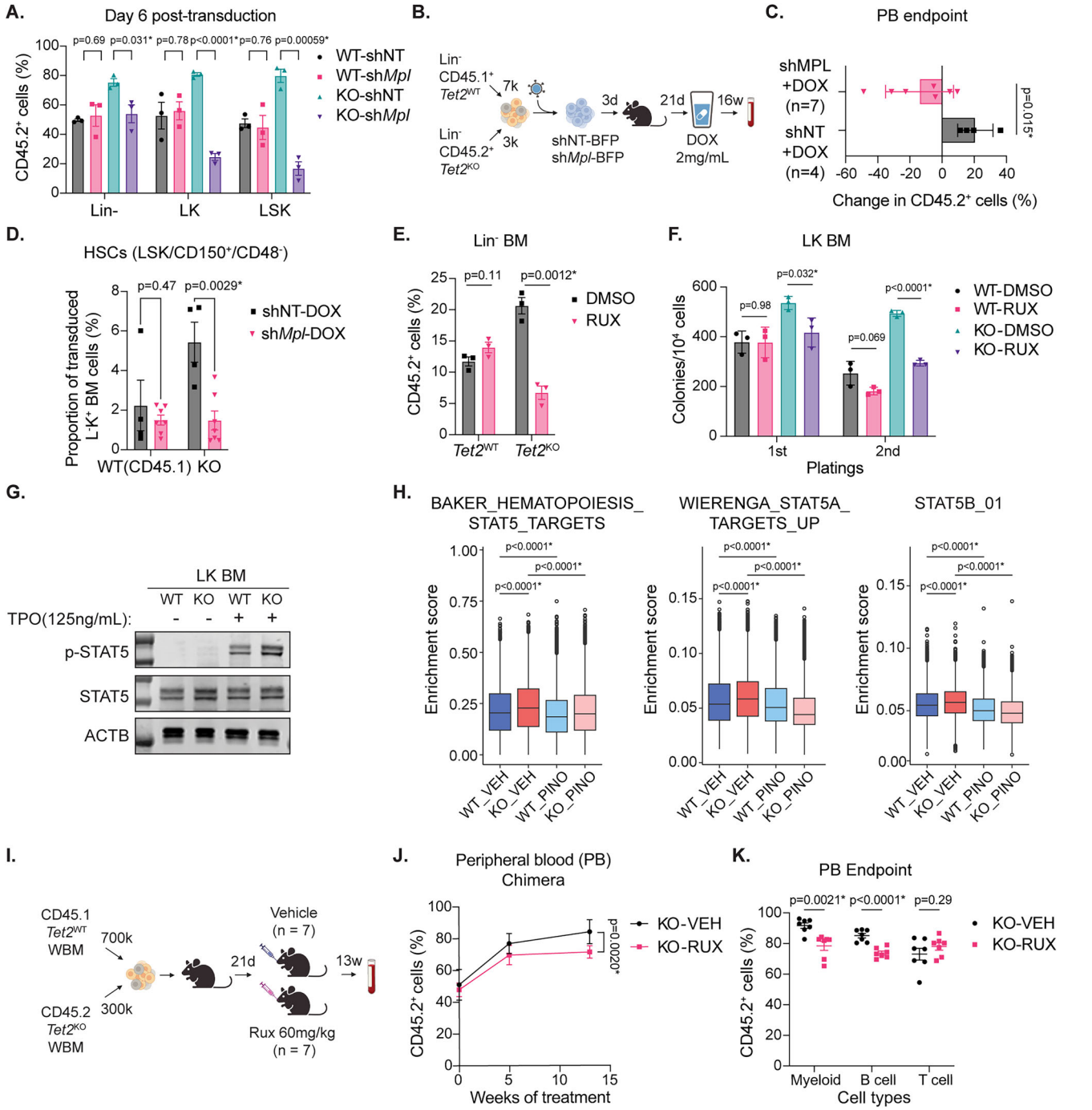

Fig. 4 | Inhibition of the TPO-R/JAK/STAT signaling axis suppresses clonal expansion of *Tet2*^{KO} mouse and human HSPCs. A Percentage of BFP$^+$ CD45.2$^+$*Tet2*^{KO} or *Tet2*^{WT} BM in competition with CD45.1$^+$*Tet2*^{WT} cells at day 6 of plating. Data shown are mean ± SD. Unpaired t test used for significance. $n = 3$ experimental replicates. **B** Schematic diagram of the in vivo competition experiment evaluating the effect of *Mpl* knockdown on the competitive advantage of *Tet2*^{KO} HSPCs. Created in BioRender[85]. **C** Change in the percentage of CD45.2$^+$*Tet2*^{KO} cells in BFP$^+$ peripheral blood cells from baseline to 17 weeks after doxycycline administration. $n = 4$ for shNT and $n = 7$ for sh*Mpl*. Data are shown as mean ± SEM. Unpaired t test used for significance. **D** Percentage of HSCs in transduced LK BM of *Tet2*^{WT} (CD45.1) or *Tet2*^{KO} cells at the endpoint. Data are shown as mean ± SEM. Unpaired t test used for significance. **E** Percentage of CD45.2$^+$*Tet2*^{WT} or CD45.2$^+$*Tet2*^{KO} HSPCs in competition with CD45.1$^+$*Tet2*^{WT} HSPCs after treatment with DMSO or ruxolitinib (1 μM) for 6 days. Data are shown as mean ± SD. Unpaired t test used for significance. $n = 3$ experimental replicates. **F** Number of colonies in media supplemented with DMSO (0.01%) or ruxolitinib (RUX, 1 μM). Data are shown as mean ± SD. Unpaired t test used for significance. $n = 3$ experimental replicates. **G** Western blot showing phosphorylated STAT5 (pSTAT5) levels in *Tet2*^{WT} (WT) and *Tet2*^{KO} (KO) LK BM with (+) or without (-) TPO stimulation. **H** AUC enrichment scores of LK BM cells from each genotype and treatment group for STAT5 target gene sets. The lower and upper hinges of the box represent the 25th and 75th percentiles, and the whiskers extend to the minimum and maximum values within 1.5 times the interquartile range. The median value is depicted by the line within the box. Unpaired t test used for significance. **I** Schematic diagram of the in vivo competition experiment evaluating the effect of ruxolitinib treatment on the competitive advantage of *Tet2*^{KO} HSPCs. Created in BioRender[86]. **J** Percentage of CD45.2$^+$*Tet2*^{KO} cells in peripheral blood from baseline to the indicated time points. $n = 7$ per treatment group. Data are shown as mean ± SEM. Unpaired t test used for significance. **K** Percentage of CD45.2$^+$*Tet2*^{KO} cells in peripheral blood samples at the endpoint. Data are shown as mean ± SEM. Unpaired t test used for significance. Asterisks indicate statistical significance. Source data are provided as a Source Data file.

https://doi.org/10.1038/s41467-025-57614-y

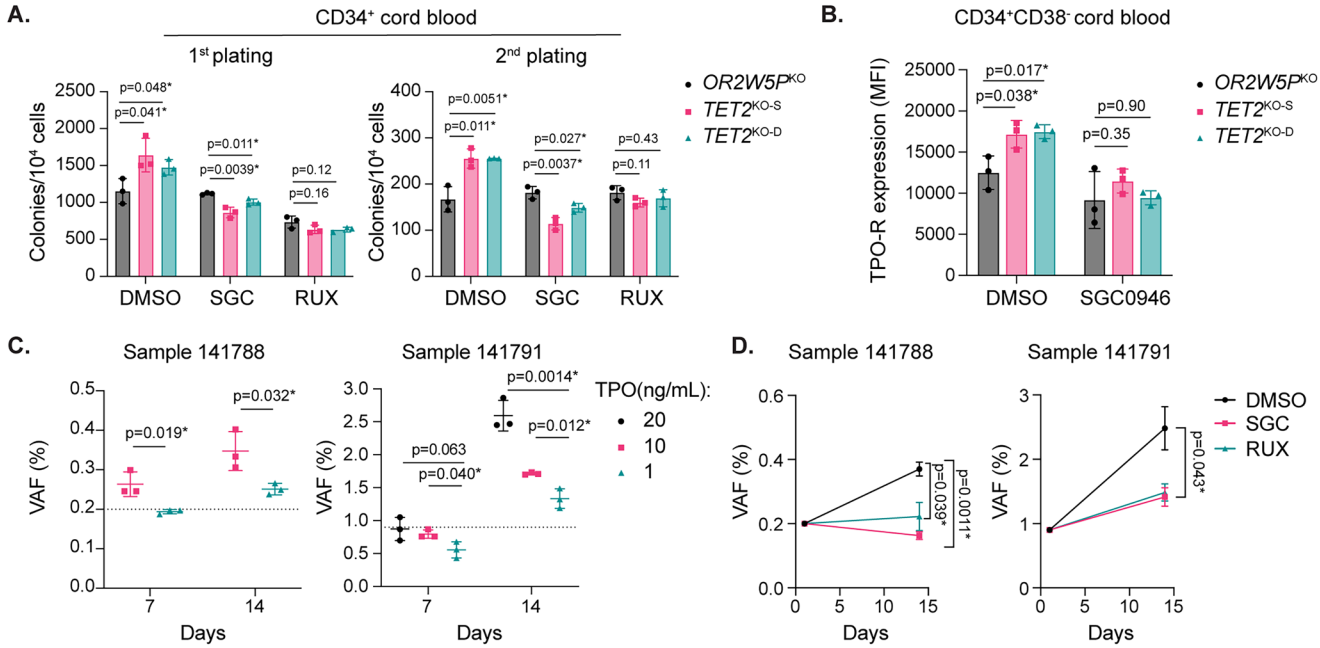

Fig. 5 | DOT1L inhibition suppresses human *TET2* mutated CHIP. A Number of colonies formed per 1×10^4 CD34$^+$ cells with Cas9-mediated knockout in *OR2W5P* or *TET2* (KO-S or KO-D) in methylcellulose containing DMSO, SGC0946 (SGC) at 1 μM, or ruxolitinib (RUX) at 0.5 μM. Unpaired t test used for significance. **B** Median fluorescent intensity (MFI) of TPO-R staining minus MFI of isotype control staining on CD34$^+$CD38$^-$ cord blood cells at 9 days after nucleofection with Cas9 RNPs targeting *OR2W5P* or *TET2*. Cells were treated with DMSO or SGC0946 for 7 days prior to analysis. Unpaired t test used for significance. **C** Variant allele frequency (VAF) of *TET2* mutations in HSPCs enriched from mPB samples cultured in different TPO concentrations for the indicated number of days. Unpaired t test used for significance. **D** VAF of *TET2* mutations in HSPCs from mPB samples cultured with DMSO, SGC0946 at 1 μM, or ruxolitinib at 0.5 μM on day 1 and 14 ($n = 3$). Unpaired t test used for significance. Data shown are mean ± SD unless otherwise indicated. Asterisks indicate statistical significance. Source data are provided as a Source Data file.

Tet2^{KO} Lin$^-$ BM cells to a level comparable to that of *Tet2*^{WT} cells (Supplementary Fig. 4G). Drug treatment also decreased the proportion of CD45.2$^+$ *Tet2*^{KO} cells across stem and progenitor cell fractions in the BM compared with vehicle treatment (Supplementary Fig. 4H, I). Consistent with these findings, ruxolitinib treatment reduced the proportion of CD45.2$^+$ *Tet2*^{KO} cells in total PB cells and specifically in the B220$^+$ B cell and CD11b$^+$ myeloid cell fractions relative to vehicle treatment (Fig. 4J, K). These findings along with results of the *Mpl* knockdown studies above provide evidence that TET2-deficient HSPCs are dependent on signaling through the TPO-R/JAK2 signaling axis to maintain their competitive advantage.

To determine the potential relevance of our findings in humans, we used CRISPR/Cas9-mediated gene editing to knockout *TET2* in Lin$^-$ human cord blood cells. This approach has been used to model the effects of TET2 loss in human HSPCs, demonstrating increased competitive advantage and myeloid lineage bias[20,70]. We designed two sets of multi-guide guide RNAs (gRNAs) targeting *TET2* (designated "KO-S" and "KO-D") and a negative control targeting a pseudogene, *OR2W5P*. The gRNAs were complexed with recombinant SpCas9 and delivered into Lin$^-$ cord blood cells using nucleofection, reproducibly resulting in an indel efficiency over 80% in all the cell pools (Supplementary Fig. 5A, B). The proportion of cells expressing the myeloid markers, CD11b and CD14, was less in the two *TET2*^{KO} cell pools than in control cells at day 21 after nucleofection (Supplementary Fig. 5C). CD34 enriched *TET2*^{KO} cells also demonstrated a higher clonogenic potential than control cells (Fig. 5A). These findings confirm the known impact of TET2 deficiency on self-renewal and differentiation of HSPCs. Importantly, the expression of TPO-R was higher in the CD34$^+$CD38$^-$ fraction of *TET2*^{KO} cells than in control *TET2*^{WT} cells, an effect that was reversed by DOT1L inhibition (Fig. 5B, Supplementary Fig. 5D, E). The proportion of TPO-R$^+$ cells in the immunophenotypic HSC (CD34$^+$/CD38$^-$/CD90$^+$/CD45RA$^-$) fraction was also higher in *TET2*^{KO} cells compared with control cells (Supplementary Fig. 5D, F). Notably, the upregulation of TPO-R was not observed on CD34$^+$CD38$^+$ progenitors, as well as in CD90$^-$CD45RA$^-$ and CD90$^+$CD45RA$^+$ cells within the CD34$^+$CD38$^-$ fraction (Supplementary Fig. 5E, F). These findings suggest that the impact of TET2 deficiency on TPO-R expression may be restricted to HSCs. Treatment with DOT1L and JAK2 inhibitors preferentially reduced the clonogenic potential and viability of *TET2*^{KO} HPCs over their *TET2*^{WT} counterparts (Fig. 5A and Supplementary Fig. 5G). Finally, we assessed if attenuation of TPO-R signaling could suppress the clonal expansion of *TET2*-mutated HPCs derived from human samples with naturally acquired CH. We enriched Lin$^-$ cells from two mobilized peripheral blood (mPB) samples with each carrying at least one predicted *TET2* loss-of-function mutation (Supplementary Fig. 5H). The purified cells were cultured in TPO-containing medium, and the size of the mutant clones at different time points was monitored using sample-specific TaqMan genotyping probes and droplet digital PCR (ddPCR). A lower TPO concentration and treatment with SGC0946 or ruxolitinib decreased the rate of expansion of *TET2*-mutated clones (Fig. 5C, D). Our findings demonstrate that human *TET2*-mutated HPCs express higher levels of TPO-R and are dependent on TPO-R signaling to sustain their competitive advantage.

Discussion

Our findings demonstrate that TET2-deficient HSPCs are dependent on TPO-R signaling to outcompete their *TET2*^{WT} counterparts. This differential dependency is mediated through aberrant DOT1L-mediated H3K79 methylation of the *Mpl* locus, leading to an increase in the proportion of *Mpl*-expressing HSCs. *Mpl*$^+$ HSCs have a more primitive transcriptional profile and are endowed with the ability to respond to TPO stimulation. We further showed that inhibition of DOT1L or the TPO-R/JAK2 signaling axis is effective in suppressing the competitive advantage of *TET2*-mutated HSPCs, thus identifying tractable therapeutic targets against *TET2* mutation-driven CH.

Although TET2 deficiency has been shown to increase the stemness properties of HSCs, the underlying mechanisms remain unclear[13,16]. Our data indicate that aberrant expression of *Mpl* in the HSC compartment may be a fundamental driver of this effect. We propose a model in which TET2 deficiency increases the overall stemness potential of mutant HSCs by expanding the proportion of Mpl^+ cells. Previous studies have shown that Mpl^+ HSCs possess greater long-term repopulating capacity relative to Mpl^- HSCs in murine and human systems[54,71]. Moreover, we showed that the transcriptomes of Mpl^+ HSCs were enriched for gene signatures associated with stemness, indicative of their more primitive state. Notably, we observed that TET2 deficiency did not further upregulate the expression of stemness-related genes in the Mpl^+ fraction of HSCs, indicating the impact of TET2 deficiency on stemness is primarily mediated through modulation of TPO-R signaling. In addition to the direct impact of TPO-R signaling on mutant HSCs, it may also indirectly enhance their relative fitness by conferring resistance to the suppressive effects of pro-inflammatory cytokines such as tumor necrosis factor alpha (TNF-α)[72].

Although DOT1L has been shown to be essential for normal hematopoiesis and the maintenance of mixed lineage leukemia (MLL)-rearranged leukemias[25,73,74], a requirement for DOT1L activity in the expansion of *TET2*-deficient HSPCs has not previously been reported. Our study showed that while TET2 deficiency did not cause global changes in H3K79 methylation, it was associated with locus-specific changes, revealing a connection between TET2 and this epigenetic mark. Specifically, we found that the level of H3K79me2 was higher at the *Mpl* locus in *Tet2*-mutated HPCs. The precise mechanisms by which TET2 deficiency leads to these locus-specific changes are unclear. We speculate that TET2 might bind directly or indirectly via other interacting proteins to DOT1L or lysine demethylase 2B (KDM2B)[75], a H3K79 demethylase, and its loss could lead to aberrant localization of one or both epigenetic modifiers, resulting in locus-specific changes in H3K79 methylation levels. Another potential mechanism might involve a crosstalk between the 5-mC/5-hmC and H3K79 methylation mark, whereby locus-specific changes in 5-mC/5-hmC due to TET2 deficiency cause localized alterations in H3K79 methylation. Further studies are required to delineate the precise link between TET2 and DOT1L activity.

The presence of CHIP is associated with an increased risk of a growing list of hematologic malignancies and age-related illnesses[76,77]. Interventions that effectively suppress the expansion of mutant HSCs can potentially lower the risk of CHIP-associated adverse outcomes and positively impact the health of a large segment of the aging population. Our findings here identify DOT1L and the TPO-R/JAK2 signaling axis as potential therapeutic targets against *TET2* mutation-driven CHIP.

There are several limitations of the study. First, our study was focused on identifying dependencies associated with *TET2* mutations. It is unclear if the observed dependencies on DOT1L activity and TPO-R signaling are specific for *TET2* mutations or shared across other CH driver mutations. It is conceivable that mutations affecting functionally different genes in CH share common pathogenic mechanisms and dependencies with *TET2* mutations. Second, the HPC^{HOXB4} cell lines and unmodified BM HPCs were cultured in supra-physiologic level of cytokines including stem cell factor (SCF), fms-like tyrosine kinase (FLT3) ligand, and TPO. Although these cytokines are routinely used to maintain murine and human HSPCs ex vivo[78–80], they may create an environment that augments the competitive advantage of $Tet2^{KO}$ cells beyond what naturally occurs in vivo. To address this concern, we conducted in vivo competitive transplantation assays, demonstrating the advantage of $Tet2^{KO}$ cells in a physiologically relevant setting. We also showed that this advantage could be suppressed by inhibiting DOT1L activity and TPO-R signaling. Third, the HPC^{HOXB4} cell lines and in vitro culture conditions used are not suitable for modeling the myeloid differentiation bias associated with TET2 mutations. Lastly, although a larger clone size has generally been associated with a higher risk of developing hematologic malignancies and other CHIP-related illnesses, it is not known if the suppression of clonal expansion alone is sufficient to decrease the risk of these adverse outcomes[6,7,81–83]. There are limitations to current in vitro assays and animal models to vigorously test this hypothesis. Clinical trials involving interventions that suppress the expansion of mutant clones in CHIP carries are ultimately required to address this important clinically relevant question.

Methods

Mouse models

$Tet2^{KO}$ (strain name: B6(Cg)-$Tet2^{tm1.2}$Rao/J) parental mice were ordered from the Jackson Laboratory and crossed with $Tet2^{WT}$ C57BL/6 J mice to heterozygous ($Tet2^{HET}$) mice. The $Tet2^{HET}$ mice were then crossed to generate $Tet2^{WT}$ and $Tet2^{KO}$ animals in the same litter. CD45.1$^+$ $Tet2^{WT}$ mice in the C57BL/6 J background (strain name: B6.SJL-Ptprca Pepcb/BoyJ) were ordered from the Jackson Laboratory.

Generation of the HPC^{HOXB4} cell models

Bone marrow cells were isolated from 8-week-old male $Tet2^{WT}$ and $Tet2^{KO}$ littermates from a $Tet2^{HET}$ x $Tet2^{HET}$ breeding pair. Sca-1$^+$ HSPCs were enriched using the EasySep™ mouse SCA1 positive selection kit (STEMCELL, #18756). Enriched cells were then infected with retroviral particles expressing HOXB4-Venus (a gift from Norman Iscove's lab). Briefly, $Tet2^{WT}$ or $Tet2^{KO}$ cells were seeded at a density of $2x10^5$ cells/mL in a well in a 24-well TC-treated tissue culture plate (Falcon, #353047) and infected with 50uL of viral supernatant diluted in 450uL of growth medium (see 'Tissue culture' section) in the presence of 8ug/mL of polybrene (Millipore, #TR10039). Growth medium was replaced on the next day. The level of Venus fluorescence was measured by flow cytometry at 72 hours post infection to access transduction efficiency.

Human mobilized peripheral blood (mPB) samples

Human mPB samples were obtained with informed consent from Princess Margaret Cancer Centre following the procedures approved by the University Health Network (UHN) research ethic board. Mononuclear cells were isolated by density gradient centrifugation using Ficoll-Paque™ (Fisher Scientific, #45001749), and hematopoietic progenitors were enriched through lineage marker depletion (STEMCELL, #14056).

Human cord blood samples

Human cord blood samples were obtained with informed consent from Princess Margaret Cancer Centre following the procedures approved by the University Health Network (UHN) research ethic board. Mononuclear cells from 1-5 pooled female and male donors were isolated and enriched for HSPCs using the above-mentioned protocols.

Tet2 genotyping

Genomic DNA was extracted from mouse tails and the HPC^{HOXB4} cell lines using standard protocols. Genotyping PCR was performed according to the protocol provided by the Jackson Laboratory for B6(Cg)-$Tet2^{tm1.2}$Rao/J mice. The sequence of the primers used are shown in Supplementary Table 1. Genotyping PCR was conducted using Taq polymerase (NEB, #M0495S) and buffer (ThermoFisher, #18067017). PCR products were visualized on 1.5% (w/v) agarose gels with SYBR™ Safe DNA gel stain (Thermo Scientific, #S33102).

Tissue culture

HPC^{HOXB4} cells were cultured in IMDM medium (Wisent, #319-105-CL) containing 10% FBS (Wisent, #080-150), murine stem cell factor (mSCF, 100 ng/mL; STEMCELL, #78064.2), recombinant human FLT3 ligand (FLT3-L, 50 ng/mL; STEMCELL, #78009.2), and recombinant human thrombopoietin (TPO, 25 ng/mL; STEMCELL, #78210.2).

Hematopoietic progenitor cells were isolated from human mPB samples using the EasySep™ human progenitor cell enrichment kit (STEMCELL, #19356) and cultured in StemSpan SFEM II medium (STEMCELL, #09655) supplemented with 20% BIT 9500 (STEMCELL, #09500), 1% Gluta-Plus (Wisent, #609-066-EL), mSCF (100 ng/mL), FLT3-L (100 ng/mL), TPO (62.5 ng/mL), StemReginin/SR1 (750 nM, SelleckChem, S2858), and UM729 (500 nM, STEMCELL, #72332).

Cord blood hematopoietic progenitor cells were isolated from cord blood samples using the EasySep™ human progenitor cell enrichment kit (STEMCELL, #19356) and cultured in StemSpan SFEM II medium (STEMCELL, #09655) supplemented with 20% BIT 9500 (STEMCELL, #09500), 1% Gluta-Plus, mSCF (100 ng/mL), FLT3-L (100 ng/mL), TPO (62.5 ng/mL), StemReginin/SR1 (750 nM, SelleckChem, S2858), and UM729 (500 nM, STEMCELL, #72332).

All cell lines and human samples were maintained in an incubator at 37 °C with 5% CO_2.

Lentivirus production and transduction

HEK293T cells were grown in RPMI 1640 medium (Wisent, #350-035-CL) supplemented with 10% FBS (Wisent, #080-150) and 1% Gluta-Plus (Wisent, #609-066-EL). Cells were seeded in 15 cm tissue culture plates (Sarstedt, #83.3903) at a density of 7×10^6 cells per plate one day before transfection. On the day of transfection, cells were co-transfected with lentiviral plasmid vectors, psPAX2 (Addgene, #12259), and pCMV-VSVG (Cell biolabs, #320023) using the jetPRIME transfection reagent (Polyplus, #CA89129-924) according to manufacturer's protocol. Supernatant containing viral particles was collected at 48- and 72-hours post transfection and filtered through a 0.45 μm PVDF membrane (Sigma, #SE1M003M00). Viral particles were precipitated in 40% (w/v) polyethylene glycol (Sigma, #89510-1KG-F) overnight. On the next day, the viral particles were collected by centrifugation at 3,248 g for 30 mins at 4 °C. The pellet was resuspended in HBSS (Gibco, #14170112) + 25 mM HEPES (Thermo Fisher, #15630-080) and stored at −80 °C for long term storage.

For lentiviral transductions, non-TC-treated 24 well plates were coated with 20 μg/mL of Retronectin (Takara, Cat # T100B) for 2 hours at room temperature followed by aspiration and blocking with PBS containing 2% (w/v) BSA (Wisent Bioproducts, Cat # 800-096-EG) for 30 mins at room temperature. After aspiration of the blocking buffer, the concentrated virus suspension was added to wells. The plates were then centrifuged at 3248 g for two hours at 4 °C to allow virus binding. Following centrifugation, unbound virus was aspirated, and cells were added. The plates were then transferred to a 37 °C incubator to initiate lentiviral infection.

Generation of Venus$^-$ cells using CRISPR/Cas9

A synthetic sgRNA targeting Venus was ordered from Synthego. See Supplementary Table 2 for sequence. Recombinant *S.pyogenes* Cas9 endonuclease at a concentration of 10ug/uL (62uM) was purchased (IDT, #1081058). The sgRNA was reconstituted in 15uL of TE buffer to reach a stock concentration of 0.1 mM. 2.5uL of the sgRNA was then mixed with 1.5uL of SpCas9 in a final volume of 25uL of Lonza P3 nucleofection solution (Lonza, #V4XP-3024) and incubated at room temperature for 15 minutes to allow formation of the sgRNA/Cas9 RNP complex. 1x10^6 *Tet2*^{WT}HPC^{HOXB4} cells were resuspended in 75uL of P3 nucleofection solution, added to the sgRNA/Cas9 RNP complex, and transferred to a Lonza nucleofection microcuvette. Nucleofection was conducted using a Lonza Amaxa™ 4D-Nucleofector under the program CA137. The presence of Venus knockout (Venus$^-$) cells was assessed by flow cytometry 4 days after nucleofection.

In vitro competition assays

Competition assays were conducted in 96-well round-bottom tissue culture plates (Sarstedt, #83.3925) with a total of 1×10^4 cells seeded in each well.

For competition assays involving HPC^{HOXB4} cells, BFP$^-$ or Venus$^+$ HPC^{HOXB4} cells were mixed with BFP$^+$ or Venus$^-$ competitor cells, respectively, at a 1:4 starting ratio in HPC^{HOXB4} growth medium to start the competition. BFP$^+$ competitor cells were generated by transducing *Tet2*^{WT}HPC^{HOXB4} cells with the pRSI9-U6-sh-UbiC-TagBFP-2A-puro vector (Addgene, #28289). Venus$^-$*Tet2*^{WT} HPC^{HOXB4} competitor cells were generated as above. The BFP$^+$ and Venus$^-$ competitor cells were sorted to >99% purity using a Becton Dickinson Aria III CFI cell sorter.

For competition assays involving unmodified murine bone marrow HSPCs, CD45.2$^+$ and CD45.1$^+$ whole bone marrow cells were harvested from age-matched mice (10–15 weeks). Lin$^-$Kit$^+$ bone marrow HSPCs were enriched using the EasySep mouse hematopoietic progenitor isolation kit (STEMCELL, #19856) followed by the c-KIT positive enrichment kit (STEMCELL, #18757). Enriched CD45.2$^+$ and CD45.1$^+$ cells were then mixed at a 1:4 starting ratio and cultured in MethoCult™ GF M3434 medium (STEMCELL, #03434) supplemented with recombinant human TPO (25 ng/mL).

Chemical library screen

Epigenetic probes were dissolved in DMSO to achieve a 20,000X stock solution and then diluted in PBS to achieve a 200X working stock solution. BFP$^+$*Tet2*^{WT}HPC^{HOXB4} was generated by lentiviral transduction of *Tet2*^{WT}HPC^{HOXB4} with a pCDH-EF1-TagBFP-T2A vector and enriched by FACS sorting. BFP$^-$*Tet2*^{KO}HPC^{HOXB4} cells were mixed with BFP$^+$*Tet2*^{WT}HPC^{HOXB4} competitor cells at the ratio of 1:4 and then seeded in 96-well round-bottom TC-treated plates at 1×10^4 total cells per well. The cells were cultured in HPC^{HOXB4} growth medium and treated with each epigenetic probe at a final concentration shown in Supplementary Table 3 or DMSO (0.01%). Cells were split at 1:10 ratio on day 7 by adding 20uL of cells from old wells to 180uL of media containing epigenetic probes at screen concentration. The percentage of BFP$^+$ cells in each well was measured by flow cytometry after 14 days of treatment.

Flow cytometry

For staining of cell surface antigens, cells were incubated with antibodies at the recommended dilutions (Supplementary Table 4) in FACS buffer (HBSS supplemented with 2% FBS and 0.1% sodium azide) for 20 mins at 4 °C. The cells were washed once in FACS buffer prior to analysis. For Annexin V staining, cells were resuspended in Annexin V buffer and stained with APC-conjugated Annexin V diluted in 1:200 (Invitrogen, #A35110) for 15 mins at room temperature prior to analysis. Flow cytometry analysis was conducted using the Beckman Coulter CytoFLEX analyzer.

FCS files were analyzed using the FlowJo™ V10 software.

Intracellular flow cytometry

Intracellular flow cytometry staining for phospho-STAT5 in murine bone marrow cells was performed using the BD Cytofix/Cytoperm fixation and permeabilization kit according to the manufacturer's protocol. Briefly, fixed and permeabilized cells were stained with a phospho-STAT5 antibody (CST, #9359) diluted 1:200 in HBSS supplemented with 2% FBS and 0.1% sodium azide for 1 hour at room temperature. The cells were then washed in FACS buffer and stained with an Alexa Fluor 647-conjugated anti-rabbit IgG (H + L) secondary antibody (CST, #4414S) diluted 1:2,000 in PBS with 1% FBS and 50 mM EDTA for 30 mins at room temperature. A rabbit IgG isotype antibody (CST, #2985S) was used to determine the level of isotype control staining.

EdU proliferation assay

One day prior to the assay, drug-treated *Tet2*^{WT} and *Tet2*^{KO} HPC^{HOXB4} cells were seeded in wells in a 24-well tissue culture plate at a cell density of 1×10^5 cells/mL. On the next day, EdU dissolved in DMSO was directly added to the growth medium at a final concentration of 10uM.

The cells were incubated with EdU for 1 hour at 37 °C prior to staining. Staining for EdU incorporation was performed using the Click-iT Pacific Blue EdU flow cytometry assay kit (Invitrogen, #C10636) as per the manufacturer's protocol.

Colony-forming unit (CFU) assays

$CD34^+$ human HSPCs were enriched from cord blood samples using the $CD34^+$ positive selection kit (STEMCELL #17856). 1×10^4 enriched LK murine HSPCs or $CD34^+$ human HSPCs were resuspended in 1.1 mL of MethoCult™ GF3434 medium or MethoCult™ H4435 medium, respectively. The medium was supplemented with recombinant human TPO (25 ng/mL). The resuspended cells were added to wells in a 6-well tissue culture plate. The number of colonies formed was determined after 7 days (mouse) or 10 days (human) in culture. Cells were replated every 7 days for mouse bone marrow and every 14 days for human HSPCs.

RNA-sequencing analysis

Total RNA was extracted from cells using the Qiagen RNeasy plus kit (Qiagen, #74134) and quantified using a Nanodrop spectrophotometer. All samples had a RIN value greater than 9. Samples were submitted to Novogene Corporation for sequencing analysis. Library construction, sequencing, and processing of sequencing data were done by Novogene following their standard pipeline. Sequencing was performed on an Illumina NovaSeq 6000 system. Reads containing adaptors and low-quality reads with Phred scores less than 33 were filtered. Clean reads were then mapped to the reference genome using the STAR software v2.6.1 d. Quantification of mapped reads was conducted on FeatureCounts (v1.5.0-p3) program and default parameters were applied.

For differential gene expression (DGE) analysis, triplicate pairwise samples were analyzed using DESeq2 R package (v1.20.0). P-values were attained by the Wald test and adjusted using Benjamini and Hochberg's approach. $|\log2FC| > 1.5$ and padj <0.01 were used as the cutoffs for differentially expressed genes.

Site-specific H3K79 methylation by dCas9-DOT1L

sgRNAs targeting the promoter and gene body of *Mpl* (Supplementary Table 5) were cloned into pRSI9-U6-scaffold-TagRFP-T2A-puro backbone and mixed following midiprep (GenebBio system, #FAFTE 002-1G-10). Lentivirus was prepared using the mixed plasmid containing equal concentration of each guide following the protocol above. *Tet2*^{WT} HPC^{HOXB4} cells were transduced with the lentivirus and positively selected with 1ug/mL puromycin (InvivoGen, #ant-pr-1) for five days. dCas9-DOT1L vector was delivered into the cells through nucleofection at the concentration of $0.5ug/10^5$ cells using Lonza P3 nucleofection kit (Lonza # V4XP-3032) under the protocol CA137. Cells were harvested after 48 and 72 hours and total mRNA was extracted for assessing *Mpl* gene expression. qPCR primers were listed in Supplementary Table 6.

Chromatin-immunoprecipitation sequencing (ChIP-seq) analysis

Cells were fixed with 1% formaldehyde (Thermo Scientific, #410730050) according to the Active Motif ChIP cell fixation protocol. Fixed cell pellets were submitted to Active Motif for ChIP-seq analysis. Briefly, 15ug of chromatin and 10uL of H3K79me2 antibody (Active Motif, #39143) were used for each IP reaction. Illumina base-call data were processed and demultiplexed using bcl2fastq2 v2.20 and low-quality bases with Phred scores less than 33 were trimmed. 75 bp single-end sequence reads were subsequently mapped to the genome through BWA v0.7.12 algorithm with default settings. Low quality reads were filtered out and PCR duplicates were removed. Aligned sequencing reads, or tags, were extended to 200 bp from the 3′ end, followed by dividing the genome into 32 bp bins and counting the number of fragments in each bin. Determination of enriched regions was done using SICER 1.1 peak calling tool, with FDR <1e-10 and gap parameter of 600 bp used as cutoffs. False ChIP-seq peaks as defined within the ENCODE blacklist were removed. Differential methylation analysis was conducted using DiffBind R package version 3.10.0 and signals from each sample were normalized to library size. P-values were attained by the Wald test and adjusted using Benjamini and Hochberg's approach. Hypermethylated regions in pairwise comparisons were defined using log2(FC in normalized reads) >1.5 and padj (FDR) <0.01 as cutoffs. Hypomethylated regions were defined using log2(FC in normalized reads) < −1.5 and padj (FDR) <0.01 as cutoffs. Differentially methylated genes were defined as genes with at least one region passing the above thresholds. Average peak signals from two replicates of each sample were obtained through randomly sampling 50 percent of reads from the corresponding BAM file of each replicate and merged using Samtools version 1.14. Average plots and heatmaps were generated using Deeptools version 3.5.1. BigWig files were visualized using WashU Epigenome browser.

RT-qPCR

Total RNA was extracted from cells using the Qiagen RNeasy plus kit and quantified on a Nanodrop spectrophotometer. Reverse transcription and quantitative PCR were performed using the Luna® Universal One-step RT-qPCR kit (NEB, #E3005S) and the Bio-Rad CFX touch real-time PCR detection system. The primers used are listed in Supplementary Table 6. The threshold cycle (Ct) value was determined using CFX Manager v3.1. Gene expression was calculated using the $^{\Delta\Delta}$Ct method. Ct values were normalized to beta actin (*Actb*).

ChIP-qPCR

Lin^-Kit^+ bone marrow HSPCs were enriched from *Tet2*^{WT} and *Tet2*^{KO} mice using selection kits (STEMCELL, #19856 and #18757). Chromatin for each CHIP reaction was prepared with 10^6 HSPCs using Diagenode chromatin EasyShear kit following the manufacturer protocol (Diagenode # C01020010). Chromatin was sheared at 4 °C on a Bioruptor® Pico sonicator in 100uL volume with 30 s on and 30 s off for 20 pulses. Each ChIP reaction was conducted using 7uL of H3K79me2 antibody (Active motif, #39143) following a published protocol (Bailey SD et al., *Nat Genet*. 2016). DNA was purified using Zymo ChIP DNA clean and concentrator (Zymo research, #D5205) and eluted in 40uL of deionized water. qPCR was performed with Biobasic qPCR mastermix (Biobasic, #QPCR004-S) and the Bio-Rad CFX touch real-time PCR detection system. qPCR primers against *Mpl* and two negative control regions were ordered from IDT. Sequences of ChIP-qPCR primers are listed in Supplementary Table 7. Enrichment was calculated using the percent input method.

Single-cell RNA (scRNA) sequencing

Whole bone marrow cells were isolated from 15 to 20-week-old *Tet2*^{WT} and *Tet2*^{KO} male littermates following red blood cell depletion. Cells from each donor were transplanted into four lethally irradiated 8-week-old CD45.2 *Tet2*^{WT} recipients at $1x10^6$ cells per animal. Following four weeks of engraftment, mice were subject to pinometostat (60 mg/kg, MCE #HY-15593) or vehicle (10% DMSO, 40% PEG300, 5% Tween-80, and 45% saline) treatment through subcutaneous injection twice a day (2 animals per cell type per treatment group) for 21 days. Mice were then euthanized and bone marrow Lin^-Kit^+ (LK) cells were enriched from the bone marrow using selection kits (STEMCELL, #19856 and #18757). The purified cells were resuspended in IMDM medium (Wisent, #319-105-CL) and subjected to library preparation using 10x Genomics Chromium Single Cell 3′ v3.1 kit and 3′ sequencing on illumina Novaseq 6000 sequencing system. The FATSQ files were processed using Cellranger v7.0.0 pipeline to generate count matrices. Cells were filtered using the following cutoffs: 200 <nFeature <9000; percent of mitochondrial reads <12.5.

The filtered reads were then normalized accounting for cell cycle difference using the SCTransform function from the Seurat package (v5.0.1). Samples showed a median of 22,504 Unique Molecular Identifiers (UMIs) per cell and 5044 genes detected.

The filtered cells were subsequently assigned with a cell type label using the previously curated gene list (Izzo et al., *Nat Genet*. 2020). HSC = Hematopoietic stem cell; IMP = Immature myeloid progenitor, Mono = Monocyte progenitor, Neu = Neutrophil/granulocyte progenitor; EB = Erythroid/basophil progenitor; Ery = Erythroid progenitor; MkP = Megakaryocyte progenitor; CLP = Common lymphoid progenitor; Ba = Basophil progenitor; Eo = Eosinophil progenitor; B-cell-P = B cell progenitor; T-cell-P = T cell progenitor. Uniform Manifold Approximation and Projection (UMAP) reduction with the following parameters: reduction = "pca", dims = 1:50 was employed for clustering.

AUCell (v1.25.0) package was used for gene signature enrichment analyses. Gene sets were imported from the molecular signatures database (MSigDB). Top 20 percent highest expressed genes were used in calculating the area under curve (AUC) for each gene set. Student's T test was used to determine significance levels between two groups.

Differential gene expression (DGE) analysis comparing *Mpl*$^{+}$ vs *Mpl*$^{-}$ HSCs from the vehicle treated group was performed using FindMarkers() function of the Seurat package. Non-paramatric Wilcoxon rank sum test was used to calculate differentially expressed genes. $|Log_2FC| > 1$ was set as the fold-change cutoff. Only genes detected in equal or more than 0.01 percent of cells were tested. Genes passing the fold-change threshold were filtered again using adjust *p* value (padj) <0.01 as cutoff. Cell type specific markers were imported from PanglaoDB (Franzén et al., *Database*. 2019) for Fig. 3I.

Western blot

Standard Western blotting techniques were performed. Blots were incubated with primary antibodies (Supplementary Table 8) diluted in 5% (w/v) BSA in TBST overnight at 4 °C on a shaking platform. On the next day, the blots were washed for five minutes for three times with TBST and incubated with a secondary antibody (LI-COR, #926-32213 or LICOR, #926-68073) at 1:2,000 dilution in 5% (w/v) BSA in TBST at room temperature for 1 hour. Membranes were washed three times again and imaged on the Odyssey CLx Imaging system (LI-COR Biosciences).

For western blot measuring TPO-stimulated pSTAT5 levels, 1 million HPC^{HOXB4} or bone marrow LK cells from *Tet2*^{WT} and *Tet2*^{KO} mice were counted and washed in PBS, and then cultured in the TPO-withdrawn growth medium (IMDM + 10% FBS, mSCF at 100 ng/mL, FLT3-L at 50 ng/mL) in a 24-well TC plate for four hours at 37 °C with 5% CO_2. TPO was added to the treatment wells at 125 ng/mL and after 15 minutes of incubation, cells were lysed in Tris-Glycine SDS Sample Buffer (Thermo Fisher #LC2676) followed by standard western blot protocol. Information regarding the primary antibodies was listed in Supplementary Table 8.

Droplet digital PCR (ddPCR)

Genomic DNA was extracted from treated cells. 125 ng of DNA was used for each ddPCR reaction. The ddPCR reaction was prepared using the Bio-Rad ddPCR Supermix (Bio-Rad, #1863010). SNP assay primers and probes were ordered from Thermofisher (Supplementary Table 9). Plates were read using a QX200 Droplet Digital PCR System (Bio-Rad). Results were analyzed using the QuantaSoft™ software.

In vivo experiments

All in vivo experiments were performed in accordance with institutional guidelines approved by the University Health Network animal care committee. Study design and data collection were in accordance with the ARRIVE guidelines. All the murine colonies were maintained in Maxbell Animal Facility at 20–22 °C with 50–60% humidity at 12 hr dark/light cycle.

For the experiment evaluating the in vivo impacts of pinometostat, CD45.2^{+} *Tet2*^{WT} or *Tet2*^{KO} BM cells from 15-week male littermates were mixed with CD45.1^{+} *Tet2*^{WT} BM cells from an age-matched male donor at 3:7 starting ratio. The mixed cells were resuspended in Opti-MEM medium and transplanted by tail vein injection into 20 8-week-old female CD45.2^{+} *Tet2*^{WT} recipients (1x10^{6} cells per mouse) conditioned with 12 Gy of irradiation, with 10 mice per group. From day 21 of transplantation, mice were randomized and subjected to pinometostat (60 mg/kg BID, MCE #HY-15593) or Vehicle (10% DMSO, 40% PEG300, 5% Tween-80, and 45% saline) treatment through subcutaneous injection twice a day for 21 days. Mice were euthanized at the end of the treatment for bone marrow flow cytometry staining and secondary transplant. For secondary transplant, bone marrow cells from the primary recipients were mixed at equal concentration and sorted for LSK cells using the antibodies listed in Supplementary Table 4 on a BD Symphony S6A cytometer. The enriched LSK cells were mixed with whole bone marrow cells from a 15-week male CD45.1^{+} *Tet2*^{WT} donor at the ratio of 5 K:500 K per recipient and transplanted into lethally irradiated female CD45.2^{+} *Tet2*^{WT} recipients by tail vein injection ($n = 5$ animals per group). The secondary recipients were not treated with pinometostat. Mice were euthanized after 3 weeks for flow cytometry analysis.

For the experiment testing the effect of ruxolitinib, CD45.2^{+} *Tet2*^{KO} BM cells from a 12-week-old male donor were mixed with CD45.1^{+} *Tet2*^{WT} BM cells from age-matched male donors at a 3:7 ratio. The mixed cells were resuspended in Opti-MEM medium and transplanted by tail vein injection into 8-week-old female CD45.2^{+} *Tet2*^{WT} recipient mice (1 x 10^{6} cells per mouse) conditioned with 12 Gy of irradiation. At day 21 post-transplantation, the mice were randomized to receive vehicle or ruxolitinib. Ruxolitinib (Supplementary Table 10) was dissolved in DMSO and then diluted in peanut oil. Mice were administered 2% DMSO in peanut oil (vehicle control) or ruxolitinib (60 mg/kg) by oral gavage twice a day.

For the experiment testing the effect of *Mpl* knockdown, lineage-depleted (Lin^{-}) BM HSPCs from a 12-week-old male CD45.2^{+}*Tet2*^{KO} mouse were mixed with Lin^{-} BM HSPCs from two age-matched CD45.1^{+}*Tet2*^{WT} male mice at a 3:7 ratio. The mixed cells were co-transduced with a pRSITE-U6-shMpl-UbiC-TagBFP-T2A-Puro or pRSITE-U6-shNT-UbiC-TagBFP-T2A-puro lentiviral vector (Supplementary Table 11). BFP^{+} cells were sorted on day 3 after transduction, resuspended in Opti-MEM, and transplanted by tail vein injection into lethally irradiated 8-week-old *Tet2*^{WT} female mice (1 × 10^{4} cells per mouse). At day 21 post-transplantation, doxycycline (Supplementary Table 10) was added into the drinking water at a concentration of 2 mg/mL to induce shRNA expression and replaced once a week.

Peripheral blood chimerism analysis

Peripheral blood samples were collected and incubated in 1X red blood cell lysis buffer (Biolegend, #420302). The RBC-depleted cells were incubated in 50uL of PBS containing a FcR blocker (Biolegend, #426103) at 1:2,000 dilution for 10 min at 4 °C and then stained with fluorophore-conjugated antibodies in FACS buffer for 20 min at 4 °C. The stained cells were washed and resuspended in FACS buffer containing Sytox™ Green (Invitrogen, #S7020) at 1:1,000 dilution prior to flow cytometry analysis.

CRISPR/Cas9 mediated knockout of *TET2* in human HSPCs

The synthetic *TET2* KO-S sgRNAs (Supplementary Table 2) were ordered from Synthego and resuspended in TE buffer to achieve a 100uM stock concentration. The synthetic *TET2* KO-D and *OR2W5P* crRNAs were ordered from Integrated DNA Technologies and resuspended in TE buffer to achieve a 200uM stock concentration. TracrRNA was purchased from IDT (IDT, #1072532). To form the

tracrRNA:crRNA complex, 1uL of each crRNA was mixed with 2uL of tracrRNA, heated at 95 °C for 5 min on a thermocycler, and cooled. To form RNPs, 1.7uL of SpCas9 was diluted in 2.1uL of pre-warmed PBS and incubated with 1.2uL of the crRNA:tracrRNA complex or 2.5uL of sgRNAs at room temperature for 15 minutes. 1uL of Cas9 electroporation enhancer (IDT, #1075915) was added to the RNP complex solution. Cord blood HSPCs were enriched and cultured for 48 hours prior to nucleofection. After culturing, 5×10^5 HSPCs were resuspended in 100uL of Lonza P3 nucleofection solution with supplement and RNP complex was added to the cells. The cells were transferred to a Lonza nucleofection microcuvette and electroporated using program DZ100 on a Lonza Amaxa™ 4D-Nucleofector. Following electroporation, 1 mL of growth medium (StemSpan SFEM II medium with 20% BIT 9500 1% Gluta-Plus, mSCF at 100 ng/mL, FLT3-L at 100 ng/mL, and TPO at 62.5 ng/mL, StemReginin/SR1 at 750 nM, and UM729 at 500 nM) was added to each microcuvette and cells were transferred to a 24-well TC plate. Cells were resuspended in fresh growth medium on the next day. The same growth medium was used before and after nucleofection. Genomic DNA was extracted 3 days after nucleofection and subjected to PCR amplification using primers listed in Supplementary Table 12. PCR products were purified through gel extraction (Qiagen #28706) and submitted for Sanger sequencing at SickKids sequencing facility. Knockout efficiency was calculated using the ICE CRISPR analysis tool (Synthego).

Statistical analysis

Data are shown as means ± SD, unless otherwise indicated. Unpaired two-tailed Student's T test was used to determine the level of significance between 2 sets of values. If needed, P-values were corrected for multiple comparisons using the Holm-Sidak method. P-values < 0.05 were considered significant. R bioinformatic analyses were conducted in R v4.3.2. Data were analyzed and visualized using the following R packages: ggplot2 (v3.5.0), ComplexHeatmap (v2.4.3), EnhancedVolcano (v1.6.0), VennDiagram (v1.7.3), ggpubr (v0.6.0), ggrepel (v0.9.4), GenomicRanges (v1.54.1), enrichR (v3.2), clusterProfiler (v4.10.0), DiffBind (v3.12.0), AUCell (v1.24.0), msigdbr (v7.5.1), Seurat (v5.0.1), DESeq2 (v1.20.0).

Gene sets were downloaded from Molecular Signatures Database (MSigDB). Gene sets used for the enrichment analyses are: GRAHAM_NORMAL_QUIESCENT_VS_NORMAL_DIVIDING_UP; EPPERT_HSC_R; PARK_HSC_VS_MULTIPOTENT_PROGENITORS_UP.

Reporting summary

Further information on research design is available in the Nature Portfolio Reporting Summary linked to this article.

Data availability

Raw and processed data from RNA-seq, ChIP-seq, and scRNA-seq analyses in this study have been deposited in Gene Expression Omnibus (GEO) under the accession code GSE264041. HPC^{HOXB4} cell lines and cloned vectors are available under a material transfer agreement with the University Health Network. Source data are provided with this paper.

References

1. Jaiswal, S. & Ebert, B. L. Clonal hematopoiesis in human aging and disease. *Science*. https://doi.org/10.1126/science.aan4673 (2019).
2. Steensma, D. P. et al. Clonal hematopoiesis of indeterminate potential and its distinction from myelodysplastic syndrome. *Blood*. https://doi.org/10.1182/blood-2015-03-631747 (2015).
3. Marnell, C. S., Bick, A. & Natarajan, P. Clonal hematopoiesis of indeterminate potential (CHIP): Linking somatic mutations, hematopoiesis, chronic inflammation and cardiovascular disease. *J. Mol. Cell Cardiol*. https://doi.org/10.1016/j.yjmcc.2021.07.004 (2021).
4. Libby, P. et al. Clonal hematopoiesis: Crossroads of aging, cardiovascular disease, and cancer: JACC review topic of the week. *J. Am. Coll. Cardiol.* **74**, 567–577 (2019).
5. Ito, S. et al. Role of Tet proteins in 5mC to 5hmC conversion, ES cell self-renewal, and ICM specification. *Nature* **466**, 1129 (2010).
6. Jaiswal, S. et al. Clonal hematopoiesis and risk of atherosclerotic cardiovascular disease. *N. Engl. J. Med.* **377**, 111–121 (2017).
7. Abelson, S. et al. Prediction of acute myeloid leukaemia risk in healthy individuals. *Nature* **559**, 400–404 (2018).
8. Genovese, G. et al. Clonal hematopoiesis and blood-cancer risk inferred from blood DNA sequence. *N. Eng. J Med*. https://doi.org/10.1056/nejmoa1409405 (2014).
9. Xie, M. et al. Age-related mutations associated with clonal hematopoietic expansion and malignancies. *Nat Med*. https://doi.org/10.1038/nm.3733 (2014).
10. Buscarlet, M. et al. Lineage restriction analyses in CHIP indicate myeloid bias for TET2 and multipotent stem cell origin for DNMT3A. *Blood* **132**, 277–280 (2018).
11. He, Y. F. et al. Tet-mediated formation of 5-carboxylcytosine and its excision by TDG in mammalian DNA. *Science*. https://doi.org/10.1126/science.1210944 (2011).
12. Ito, S. et al. Tet proteins can convert 5-methylcytosine to 5-formylcytosine and 5-carboxylcytosine. *Science*. https://doi.org/10.1126/science.1210597 (2011).
13. Moran-Crusio, K. et al. Tet2 loss leads to increased hematopoietic stem cell self-renewal and myeloid transformation. *Cancer Cell* **20**, 11–24 (2011).
14. Quivoron, C. et al. TET2 inactivation results in pleiotropic hematopoietic abnormalities in mouse and is a recurrent event during human lymphomagenesis. *Cancer Cell* **20**, 25–38 (2011).
15. Kunimoto, H. et al. Tet2 disruption leads to enhanced self-renewal and altered differentiation of fetal liver hematopoietic stem cells. *Sci. Rep.* **2**, 1–10 (2012).
16. Ko, M. et al. Ten-eleven-translocation 2 (TET2) negatively regulates homeostasis and differentiation of hematopoietic stem cells in mice. *Proc. Natl Acad. Sci. USA* **108**, 14566–14571 (2011).
17. Sauvageau, G. et al. Overexpression of HOXB4 in hematopoietic cells causes the selective expansion of more primitive populations in vitro and in vivo. *Genes Dev.* **9**, 1753–1765 (1995).
18. Cusan, M. et al. Controlled stem cell amplification by HOXB4 depends on its unique proline-rich region near the N terminus. *Blood*. https://doi.org/10.1182/blood-2016-04-706978 (2017).
19. Schiroli, G. et al. Cell of origin epigenetic priming determines susceptibility to Tet2 mutation. *Nat. Commun*. https://doi.org/10.1038/S41467-024-48508-6 (2024).
20. Huerga Encabo, H. et al. Loss of TET2 in human hematopoietic stem cells alters the development and function of neutrophils. *Cell Stem Cell* **30**, 781–799.e9 (2023).
21. Ackloo, S., Brown, P. J. & Müller, S. Chemical probes targeting epigenetic proteins: Applications beyond oncology. *Epigenetics* **12**, 378–400 (2017).
22. Yu, W. et al. Catalytic site remodelling of the DOT1L methyltransferase by selective inhibitors. *Nat. Commun.* **3**, 1288 (2012).
23. Stein, E. M. et al. The DOT1L inhibitor pinometostat reduces H3K79 methylation and has modest clinical activity in adult acute leukemia. *Blood*. https://doi.org/10.1182/blood-2017-12-818948 (2018).
24. Figueroa, M. E. et al. Leukemic IDH1 and IDH2 mutations result in a hypermethylation phenotype, disrupt TET2 function, and impair hematopoietic differentiation. *Cancer Cell* **18**, 553–567 (2010).
25. Bernt, K. M. et al. MLL-rearranged leukemia is dependent on aberrant H3K79 methylation by DOT1L. *Cancer Cell* **20**, 66–78 (2011).
26. Daigle, S. R. et al. Potent inhibition of DOT1L as treatment of MLL-fusion leukemia. *Blood* **122**, 1017–1025 (2013).

27. Cobo, I. et al. DNA methyltransferase 3 alpha and TET methylcytosine dioxygenase 2 restrain mitochondrial DNA-mediated interferon signaling in macrophages. *Immunity* **55**, 1386–1401.e10 (2022).
28. Cull, A. H., Snetsinger, B., Buckstein, R., Wells, R. A. & Rauh, M. J. Tet2 restrains inflammatory gene expression in macrophages. *Exp. Hematol.* **55**, 56–70.e13 (2017).
29. Cai, Z. et al. Inhibition of Inflammatory Signaling in Tet2 mutant preleukemic cells mitigates stress induced abnormalities and clonal hematopoiesis. *Cell Stem Cell* **23**, 833 (2018).
30. Koepp, D. M., Harper, J. W. & Elledge, S. J. How the cyclin became a cyclin: regulated proteolysis in. *Cell cycle Cell* **97**, 431–434 (1999).
31. Yokoyama, S., Takada, K., Hirasawa, M., Perera, L. P. & Hiroi, T. Transgenic mice that overexpress human IL-15 in enterocytes recapitulate both B and T cell-mediated pathologic manifestations of celiac disease. *J. Clin. Immunol.* **31**, 1038–1044 (2011).
32. Tanaka, T., Narazaki, M. & Kishimoto, T. IL-6 in inflammation, immunity, and disease. *Cold Spring Harb. Perspect. Biol.* https://doi.org/10.1101/CSHPERSPECT.A016295 (2014).
33. Nguyen, A. T. & Zhang, Y. The diverse functions of Dot1 and H3K79 methylation. *Genes Dev.* **25**, 1345–1358 (2011).
34. Vigon, I. et al. Molecular cloning and characterization of MPL, the human homolog of the v- mpl oncogene: Identification of a member of the hematopoietic growth factor receptor superfamily. *Proc. Natl Acad. Sci. USA* https://doi.org/10.1073/pnas.89.12.5640 (1992).
35. Skoda, R. C. et al. Murine c-mpl: A member of the hematopoietic growth factor receptor superfamily that transduces a proliferative signal. *EMBO J.* https://doi.org/10.1002/j.1460-2075.1993.tb05925.x (1993).
36. Takashima, S. et al. Molecular cloning and expression of a sixth type of alpha 2,8-sialyltransferase (ST8Sia VI) that sialylates O-glycans. *J. Biol. Chem.* **277**, 24030–24038 (2002).
37. Sitnicka, E. et al. The effect of thrombopoietin on the proliferation and differentiation of murine hematopoietic stem cells. *Blood* **87**, 4998–5005 (1996).
38. Yagi, M. et al. Sustained ex vivo expansion of hematopoietic stem cells mediated by thrombopoietin. *Proc. Natl Acad. Sci. USA* **96**, 8126–8131 (1999).
39. Fox, N., Priestley, G., Papayannopoulou, T. & Kaushansky, K. Thrombopoietin expands hematopoietic stem cells after transplantation. *J. Clin. Invest* **110**, 389–394 (2002).
40. Cano-Rodriguez, D. et al. Writing of H3K4Me3 overcomes epigenetic silencing in a sustained but context-dependent manner. *Nat. Commun.* **7**, 12284 (2016).
41. Katayamaa, N. et al. Role for C-MPL and its ligand thrombopoietin in early hematopoiesis. *Leuk. Lymphoma* **28**, 51–56 (1997).
42. Yoshihara, H. et al. Thrombopoietin/MPL signaling regulates hematopoietic stem cell quiescence and interaction with the osteoblastic niche. *Cell Stem Cell* **1**, 685–697 (2007).
43. Waters, N. J. et al. Exploring drug delivery for the DOT1L inhibitor pinometostat (EPZ-5676): Subcutaneous administration as an alternative to continuous IV infusion, in the pursuit of an epigenetic target. *J. Controlled Release* **220**, 758–765 (2015).
44. Satija, R., Farrell, J. A., Gennert, D., Schier, A. F. & Regev, A. Spatial reconstruction of single-cell gene expression data. *Nat. Biotechnol.* **33**, 495–502 (2015).
45. Chan, S. Created in BioRender. https://BioRender.com/a37p701 (2025).
46. Paul, F. et al. Transcriptional heterogeneity and lineage commitment in myeloid progenitors. *Cell* **163**, 1663–1677 (2015).
47. Izzo, F. et al. DNA methylation disruption reshapes the hematopoietic differentiation landscape. *Nat. Genet* **52**, 378–387 (2020).
48. Xie, J. et al. STING activation in TET2-mutated hematopoietic stem/progenitor cells contributes to the increased self-renewal and neoplastic transformation. *Leukemia* **37**, 2457–2467 (2023).
49. Li, Z. et al. Deletion of Tet2 in mice leads to dysregulated hematopoietic stem cells and subsequent development of myeloid malignancies. *Blood* **118**, 4509 (2011).
50. Graham, S. M., Vass, J. K., Holyoake, T. L. & Graham, G. J. Transcriptional analysis of quiescent and proliferating CD34+ human hemopoietic cells from normal and chronic myeloid leukemia sources. *Stem Cells* **25**, 3111–3120 (2007).
51. Park, I. K. et al. Differential gene expression profiling of adult murine hematopoietic stem cells. *Blood* **99**, 488–498 (2002).
52. Chan, S. Created in BioRender. https://BioRender.com/q16h147 (2025).
53. Kimura, S., Roberts, A. W., Metcalf, D. & Alexander, W. S. Hematopoietic stem cell deficiencies in mice lacking c-Mpl, the receptor for thrombopoietin. *Proc. Natl Acad. Sci.* **95**, 1195–1200 (1998).
54. Solar, G. P. et al. Role of c-mpl in early hematopoiesis. *Blood* **92**, 4–10 (1998).
55. Chan, S. Created in BioRender. https://BioRender.com/d01z404 (2025).
56. Ostrander, E. L. et al. Divergent Effects of Dnmt3a and Tet2 mutations on hematopoietic progenitor cell fitness. *Stem Cell Rep.* **14**, 551–560 (2020).
57. Cai, Z. et al. Inhibition of inflammatory signaling in Tet2 mutant preleukemic cells mitigates stress-induced abnormalities and clonal hematopoiesis. *Cell Stem Cell* **23**, 833–849.e5 (2018).
58. Wang, Y. et al. Tet2-mediated clonal hematopoiesis in nonconditioned mice accelerates age-associated cardiac dysfunction. *JCI Insight*. https://doi.org/10.1172/JCI.INSIGHT.135204 (2020).
59. Papathanasiou, P., Attema, J. L., Karsunky, H., Jian, X., Smale, S. T. & Weissman, I. L. Evaluation of the long-term reconstituting subset of hematopoietic stem cells with CD150. *Stem Cells* **27**, 2498–2508 (2009).
60. Ezumi, Y., Takayama, H. & Okuma, M. Thrombopoietin, c-Mpl ligand, induces tyrosine phosphorylation of Tyk2, JAK2, and STAT3, and enhances agonists-induced aggregation in platelets in vitro. *FEBS Lett.* https://doi.org/10.1016/0014-5793(95)01072-M (1995).
61. Miyakawa, Y. et al. Thrombopoietin induces tyrosine phosphorylation of Stat3 and Stat5 in human blood platelets. *Blood* **87**, 439–446 (1996).
62. Kollmann, S. et al. A STAT5B-CD9 axis determines self-renewal in hematopoietic and leukemic stem cells. *Blood* **138**, 2347–2359 (2021).
63. Escamilla Gómez, V. et al. Ruxolitinib in refractory acute and chronic graft-versus-host disease: a multicenter survey study. *BMT* https://doi.org/10.1038/s41409-019-0731-x (2020).
64. O'Shea, J. J., Kontzias, A., Yamaoka, K., Tanaka, Y. & Laurence, A. Janus kinase inhibitors in autoimmune diseases. *Ann. Rheum. Dis.* https://doi.org/10.1136/annrheumdis-2012-202576 (2013).
65. Vainchenker, W. et al. JAK inhibitors for the treatment of myeloproliferative neoplasms and other disorders. *F1000Res* **7**, 82 (2018).
66. Gozgit, J. M. et al. Effects of the JAK2 inhibitor, AZ960, on Pim/BAD/BCL-xL survival signaling in the human JAK2 V617F cell line SET-2. *J. Biol. Chem.* https://doi.org/10.1074/jbc.M803813200 (2008).
67. Wernig, G. et al. Efficacy of TG101348, a selective JAK2 inhibitor, in treatment of a murine model of JAK2V617F-induced polycythemia vera. *Cancer Cell* **13**, 311–320 (2008).
68. Mascarenhas, J. & Hoffman, R. Ruxolitinib: The first FDA approved therapy for the treatment of myelofibrosis. *Clin. Cancer Res.* **18**, 3008–3014 (2012).
69. Chan, S. Created in BioRender. https://BioRender.com/m02z991 (2025).
70. Nakauchi, Y. et al. The cell type-specific 5hmc landscape and dynamics of healthy human hematopoiesis and TET2-mutant preleukemia. *Blood Cancer Discov.* **3**, 346–367 (2022).
71. Jeong, J. J. et al. Cytokine-regulated phosphorylation and activation of TET2 by JAK2 in hematopoiesis. *Cancer Discov.* **9**, 778–795 (2019).

72. Abegunde, S. O., Buckstein, R., Wells, R. A. & Rauh, M. J. An inflammatory environment containing TNFα favors Tet2-mutant clonal hematopoiesis. *Exp. Hematol.* **59**, 60–65 (2018).
73. Feng, Y. et al. Early mammalian erythropoiesis requires the Dot1L methyltransferase. *Blood*. https://doi.org/10.1182/blood-2010-03-276501 (2010).
74. Nguyen, A. T., He, J., Taranova, O. & Zhang, Y. Essential role of DOT1L in maintaining normal adult hematopoiesis. *Cell Res* **21**, 1370–1373 (2011).
75. Kang, J. Y. et al. KDM2B is a histone H3K79 demethylase and induces transcriptional repression via sirtuin-1–mediated chromatin silencing. *FASEB J.* **32**, 5737–5750 (2018).
76. Warren, J. T. & Link, D. C. Clonal hematopoiesis and risk for hematologic malignancy. *Blood* **136**, 1599–1605 (2020).
77. Jaiswal, S. Clonal hematopoiesis and nonhematologic disorders. *Blood* **136**, 1606–1614 (2020).
78. Flores-Guzmán, P., Fernández-Sánchez, V. & Mayani, H. Concise review: ex vivo expansion of cord blood-derived hematopoietic stem and progenitor cells: basic principles, experimental approaches, and impact in regenerative medicine. *Stem Cells Transl. Med.* **2**, 830–838 (2013).
79. Dahlberg, A., Delaney, C. & Bernstein, I. D. Ex vivo expansion of human hematopoietic stem and progenitor cells. *Blood* **117**, 6083–6090 (2011).
80. Wang, Y. et al. Tracking hematopoietic precursor division ex vivo in real time. *Stem Cell Res. Ther.* https://doi.org/10.1186/S13287-017-0767-Z (2018).
81. Bolton, K. L. et al. Cancer therapy shapes the fitness landscape of clonal hematopoiesis. *Nat. Genet.* **52**, 1219–1226 (2020).
82. Dorsheimer, L. et al. Association of mutations contributing to clonal hematopoiesis with prognosis in chronic ischemic heart failure. *JAMA Cardiol.* **4**, 25–33 (2019).
83. Jaiswal, S. & Libby, P. Clonal haematopoiesis: connecting ageing and inflammation in cardiovascular disease. *Nat. Rev. Cardiol.* **17**, 137–144 (2020).
84. Chan, S. https://BioRender.com/a37p701 (2025).
85. Chan, S. https://BioRender.com/d01z404 (2025).
86. Chan, S. https://BioRender.com/m02z991 (2025).

Acknowledgements

This work is funded by a Leukemia and Lymphoma Society of Canada Blood Cancer Research Jump Start Grant (SMC), University of Toronto Medicine by Design Cycle 2 Award (SMC), and Canadian Institutes of Health Research Project Grants DCP-186319 and PJT-175186 (SMC). We thank all members from Dr. Steven Chan's lab for reading and providing advice on the manuscript; Mr. Robert Herrington from Dr. Norman Iscove lab for kindly gifting the HOXB4 retrovirus; Dr. Marianne Rots from University of Groningen for gifting the dCas9-DOT1L construct. We also thank the staff from SickKids-UHN Flow Cytometry Facility, the SickKids TCAG Sequencing Center, the UHN Bioinformatics and HPC core, the Princess Margaret Geonomics Centre, and the Max Bell Animal Resources Center for providing technical support; the patients from Princess Margaret Hospital for donating samples for this study.

Author contributions

Y.Y., A.S., S.C. & S.M.C. designed the in vitro and in vivo experiments. Y.Y. and R.V. designed the experiments using cord blood HSPCs. Y.Y., A.S., S.C., A.C.L., A.M., M.H. & D.M.A. performed the experiments and analyzed the results. Y.Y. and A.C.L. performed computational analyses and data visualization of the RNA-seq, ChIP-seq, and scRNA-seq experiments. A.S. and S.M.C. provided supervision. S.M.C. acquired the fundings. Y.Y. and S.M.C. wrote the manuscript and discussed with the co-authors above.

Competing interests

The authors declare no competing interests.

Additional information

Supplementary information The online version contains supplementary material available at https://doi.org/10.1038/s41467-025-57614-y.

Correspondence and requests for materials should be addressed to Steven M. Chan.

Peer review information *Nature Communications* thanks Hector Huerga Encabo and the other, anonymous, reviewers for their contribution to the peer review of this work. A peer review file is available.